Defense Nuclear Agency
Alexandria, VA 22310-3398

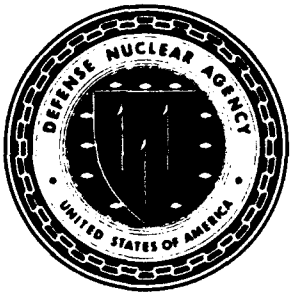

DNA-TR-93-171

Preliminary Assessment of the Importance of Turbulent Coagulation in the Kuwaiti Oil Fires

Ira Kohlberg
Institute for Defense Analyses
1801 N. Beauregard Street
Alexandria, VA 22311-1772

July 1994

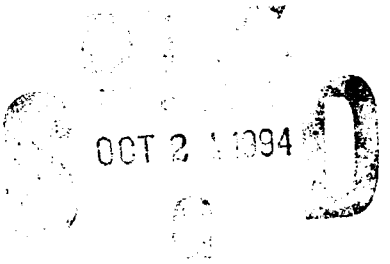

Technical Report

CONTRACT No. DNA-MIPR-92-639

Approved for public release; distribution is unlimited.

Destroy this report when it is no longer needed. Do not return to sender.

PLEASE NOTIFY THE DEFENSE NUCLEAR AGENCY, ATTN: CSTI, 6801 TELEGRAPH ROAD, ALEXANDRIA, VA 22310-3398, IF YOUR ADDRESS IS INCORRECT, IF YOU WISH IT DELETED FROM THE DISTRIBUTION LIST, OR IF THE ADDRESSEE IS NO LONGER EMPLOYED BY YOUR ORGANIZATION.

REPORT DOCUMENTATION PAGE

Form Approved
OMB No. 0704-0188

1. AGENCY USE ONLY *(Leave blank)*	2. REPORT DATE	3. REPORT TYPE AND DATES COVERED
	941001	Technical 920401 - 930630

4. TITLE AND SUBTITLE

Preliminary Assessment of the Importance of Turbulent Coagulation in the Kuwaiti Oil Fire

5. FUNDING NUMBERS

C - DNA-MIPR-92-639

6. AUTHOR(S)

Ira Kohlberg

7. PERFORMING ORGANIZATION NAME(S) AND ADDRESS(ES)

Institute for Defense Analyses
1801 N. Beauregard Street
Alexandria, VA 22311-1772

8. PERFORMING ORGANIZATION REPORT NUMBER

IDA Paper P-2854

9. SPONSORING/MONITORING AGENCY NAME(S) AND ADDRESS(ES)

Defense Nuclear Agency
6801 Telegraph Road
Alexandria, VA 22310-3398
SPWE/Cox

10. SPONSORING/MONITORING AGENCY REPORT NUMBER

DNA-TR-93-171

11. SUPPLEMENTARY NOTES

12a. DISTRIBUTION/AVAILABILITY STATEMENT

Approved for public release; distribution is unlimited.

12b. DISTRIBUTION CODE

13. ABSTRACT *(Maximum 200 words)*

This study provides a mathematical determination of the spatial distribution of aerosols due to turbulent shear coagulation and turbulent inertial coagulation, as applied to the conditions of the Kuwaiti Oil Fires (KOF) of 1991. Using an approximation from a forest fire for the normalized size distribution of aerosols, the downstream particle concentration is found by the concurrent solution of the coagulations' kinetics combined with turbulent atmospheric diffusion. The result shows the explicit dependence of the concentration on the following principal parameters: turbulent energy dissipation rate, turbulent diffusion constant, average wind speed, mass ejection from a well, Kolmogorov time scale for turbulence, and Kolmogorov length scale for turbulence. For very large values of turbulent energy dissipation rate, turbulent inertial coagulation is more effective than turbulent shear coagulation in particle growth. The spatial dependence of concentration attributed to turbulent coagulation may vary considerably. Depending on the choice of parameters, the importance of turbulent coagulation in particle transport processes may extend from less than a kilometer to tens of kilometers.

14. SUBJECT TERMS		15. NUMBER OF PAGES
Kuwaiti Oil Fires (KOF)	Turbulent Shear Coagulation	56
Particle Transport	Turbulent Inertial Coagulation	16. PRICE CODE

17. SECURITY CLASSIFICATION OF REPORT	18. SECURITY CLASSIFICATION OF THIS PAGE	19. SECURITY CLASSIFICATION OF ABSTRACT	20. LIMITATION OF ABSTRACT
UNCLASSIFIED	UNCLASSIFIED	UNCLASSIFIED	SAR

CLASSIFIED BY:

N/A since Unclassified.

DECLASSIFY ON:
N/A since Unclassified.

SUMMARY

The Kuwaiti Oil Fires (KOF) of 1991 provided an opportunity for the Defense Nuclear Agency (DNA) to address some key questions about the atmospheric transport* of particles that are relevant to the prediction of late-time dust cloud motion. During the fires, much data were collected by numerous U.S. and foreign scientific agencies, and now the critical issue is to assemble and organize a consistent set of measurements that can be evaluated against computer models to predict small particle transport. These computer models are required for the prediction of long-range transport of nuclear dust clouds and for the prediction of smoke plumes from large oil, industrial, or urban fires that might affect electro-optical sensor performance.

The KOF included features that were common with large forest fires, but the KOF also had other characteristics that made them unique. When various long-range transport codes were exercised for KOF-like problems, certain important deficiencies were encountered. This raises the following questions: Are the mathematical and physical models of the codes unsatisfactory? Are they being applied in situations for which they are not intended?

A key requirement for predicting particle transport is the necessity to follow the motion of some "tracer" particles (Lagrangian viewpoint). To be good tracers for modeling purposes, the particles must remain physically and chemically inert during the transport process. This condition of physical and chemical invariance can be termed a "frozen" or "aged" state, and it will be reached when processes such as condensation and evaporation, accretion of water vapor or other species, combustion and other chemical reactions, and turbulent coagulation are no longer active. In this paper, we evaluate turbulent coagulation. The other factors will be addressed in subsequent investigations.

The purpose of this paper is to make a preliminary assessment of the conditions under which turbulent coagulation is or is not a significant factor. Clearly, if airborne particles continue to coagulate or otherwise grow or shrink in appreciable amounts during the transport phase, they cannot be unequivocally "tagged," and this potentially diminishes

---

* In this report, transport means both advection and diffusion.

the validity of a transport calculation. The importance of this investigation is that it defines the nearest spatial region where turbulent coagulation can be neglected, so that suitable comparisons can be made between transport prediction models and experimental data (notwithstanding other aging processes).

Specific reasons for evaluating turbulent coagulation in the KOF are as follows:

- Initial reported aerosol particle/mass densities are extremely high, leading to large coagulation growth rates.
- In the large Canadian forest fire of 1950, it was found that turbulent coagulation was an important consideration.
- Mass injection into the atmosphere is comparable to or exceeds that of large forest fires.
- There is a paucity of experimental data on turbulent coagulation in the atmosphere, and it may be necessary to have a means of interpreting certain KOF experimental data in this light.
- It is important to understand the dependence of turbulent coagulation on windspeed (as it relates to transport time), turbulent kinetic energy dissipation rate per unit mass, aerosol density and size distribution, and atmospheric diffusion.
- The analytic representation of collection kernels for existing turbulent coagulation theories is based on spherical particles, but this may not be valid for KOF. Therefore, it is necessary to have a simple way of estimating the changes in coagulation dynamics as a function of aerosol shape.

The approach is to develop an analytical formulation of the spatial behavior of aerosol density as the particles are carried along the turbulent wind field while simultaneously undergoing coagulation. The KOF aerosol problem is one in which the particle density of the "superplume" is formed by the merging of hundreds of individual plumes. By example, Figure S-1 shows three individual plumes merging into a super-plume.

In this idealized figure, we hypothesize that there will be significant coagulation effects as the flames emerge from each individual well since the particle density (concentration) and mass density will be extremely high. As the individual plumes spread, the concentration will decrease by geometric dilution caused by atmospheric turbulence and coagulation. Ultimately, we postulate that the coagulation process becomes insignificant when compared to other processes due to decreasing concentrations. The surfaces that

define this transition are labeled "Coagulation Boundary." The shaded areas behind these boundaries are the regions where coagulation is assumed to be insignificant.

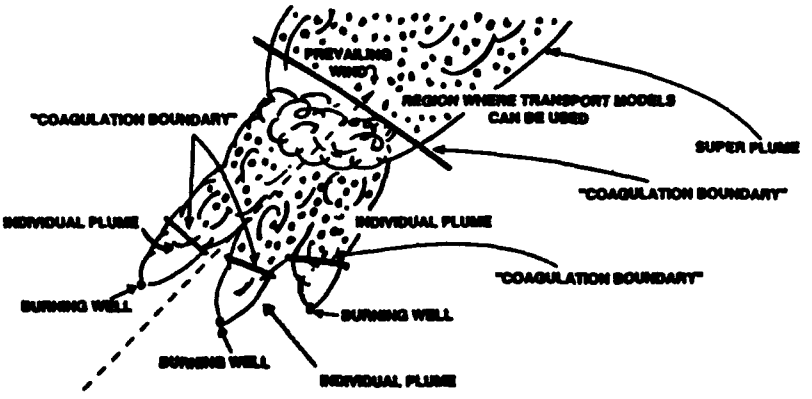

Figure S-1. Geometric viewpoint for coagulation considerations.

The first step in understanding the behavior of aerosol concentration in the superplume is to evaluate the contributions from an individual fire. Figure S-2 shows the mathematical model for a single plume. This model can be applied to an individual source or to the large plume provided that the appropriate initial conditions are present.

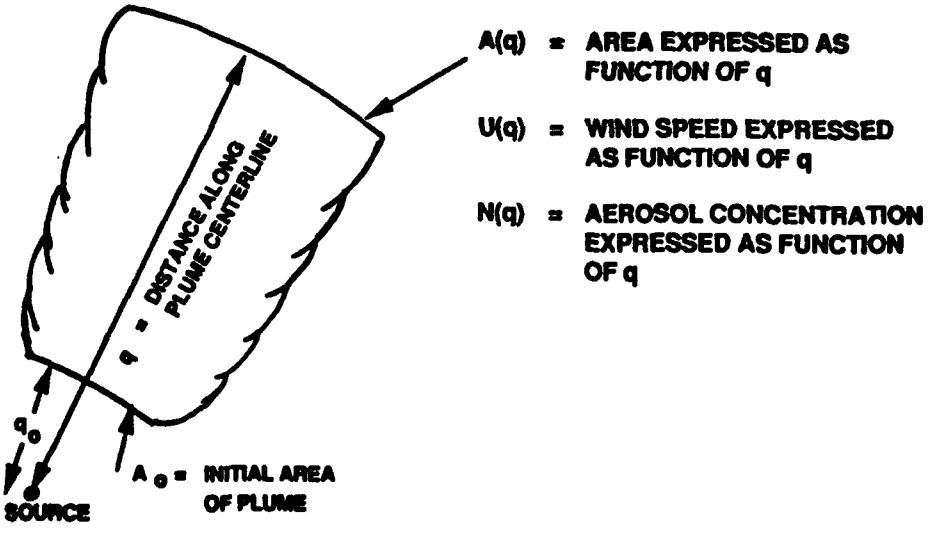

Figure S-2. Model for individual plume.

In Figure S-2, q_o is the distance from the source (oil well) where the kinetic energy of the ejected oil is no longer a factor in the transport process. $A(q_o)$ is the cross-sectional area associated with q_o. These dimensions are estimated from visual observations. From turbulent diffusion models, we obtain the approximation $A(q) = (\text{const})\ q^2$ for $q \geq q_o$. Using A(q) in conjunction with mathematical simplification of the collection kernels for turbulent shear coagulation and turbulent inertial coagulation and an approximation for the shape of the aerosol radius distribution based on the large Canadian forest fire of 1950, we have been able to derive an expression for the aerosol concentration, N(q), as a function of the turbulent dissipation rate, average windspeed, and source emission rate. For the conditions assumed in this study, turbulent inertial coagulation is nearly two orders of magnitude more effective than turbulent shear coagulation.

The concentration, N(q), along the center line trajectory of Figure S-2, is given by

$$N(q) = N_1(q)\,\Gamma_c(q) \quad , \tag{S.1}$$

where

$$N_1(q) = \frac{S_o}{U(q)\,A(q)} \tag{S.2}$$

is the ordinary geometric spreading and

$$\Gamma_c = \exp\left[-l_I\left(\frac{1}{q_o} - \frac{1}{q}\right)\right] \; ; \; q \geq q_o \tag{S.3}$$

is the part that is due to coagulation. In these equations, S_o is the particle emission rate, U(q) is the windspeed along q, A(q) is the cross-sectional area of the plume, q_o is the starting point for the growth of the plume, and l_I is a characteristic length associated with turbulent inertial coagulation. It is given by

$$l_I = \frac{5.3\,R_m r_I}{\rho_A \tau_k \lambda_k U^2} \quad , \tag{S.4}$$

where R_m is the mass emission rate, ρ_A is the atmospheric mass density, r_I is a characteristic radius associated with the aerosol size shape distribution, τ_k is the Kolmogorov time scale for turbulence, λ_k is the Kolmogorov length scale for turbulence, and U is the average windspeed.

Figure S-3 shows the general behavior of Γ_c as a function of q. The significant features of this curve are the initial value of 1.0, the asymptotic behavior $\exp(-l_I/q_o)$, and the spatial variation, which behaves as $\exp(-l_I/q)$. Turbulent inertial coagulation will not have an important effect on particle transport when this factor does not vary significantly over the range of interest (i.e., the spatial region where theoretical models of particle transport are to be compared with experimental observations).

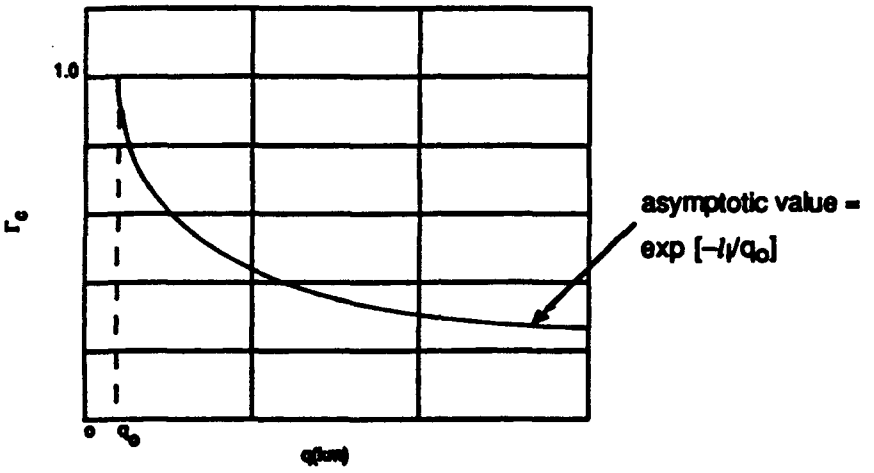

Figure S-3. Generic behavior of Γ_c as a function of q.

As shown in Figure S-3, the rate of spatial change of Γ_c decreases as the distance, q, increases. By establishing a practical criterion consistent with the prediction capabilities of particle transport codes, it is possible to establish a minimum range, q_{min}, beyond which the effects of coagulation on particle transport should not be a concern. The criterion is

$$\frac{\Gamma_c(2\,q_{min})}{\Gamma_c(q_{min})} \geq 0.9 \quad , \tag{S.5}$$

and this inequality leads to the minimum range,

$$q_{min} \geq 5\,l_I \quad , \tag{S.6}$$

in the domain of interest [where $\exp(-l_I/q_o) << 1$]. q_{min} is the distance beyond which $ln\ \Gamma_c$ changes by less than 10 percent over q_{min}.

The important point is that q_o and the factors comprising l_I can be determined from remote and in-situ measurements taken during the fires. Using estimated numbers for the conditions of the KOF, we find that l_I can range up to several kilometers and, in some cases, can be as large as 10 kilometers. On the other hand, q_o may only range up to a few hundred meters. At this time, there remains a large number of unknown factors in the computation of l_I. As the data reduction and analysis from the KOF continue, improved estimates for l_I will become available, and we will be able to define more precisely the regions where a self-consistent set of measurements can be used to validate particle transport models.

PREFACE

This paper, "Preliminary Assessment of the Importance of Turbulent Coagulation in the Kuwaiti Oil Fires," is part of a larger Defense Nuclear Agency (DNA)-sponsored program dealing with the Kuwaiti Oil Fires (KOF) of 1991. This DNA program is directed toward improving our capability to predict the transport of pollutants arising from very large natural and manmade fires.

The author has received constructive comments and support from numerous individuals in the preparation of this paper. Thanks are due to Dr. Ernie Bauer (IDA) for pointing out the importance of the fractal nature of aerosols produced in these fires and the consequences of fractal considerations in coagulation; to Dr. Ed Townsley (IDA), Dr. John Cockayne (SAIC), and LCDR Harris O'Bryant (DNA) for their critical review of the equations and mathematical formalism; to Dr. Darrel Baumgardner (NCAR) for helpful comments concerning coagulation processes and the related aerosol size distribution; to Dr. Ian Sykes (ARAP) for pointing out the relationship between time averaging and plume spreading; to Drs. Robert Oliver (IDA) and Tom Vonder Haar (METSAT) for their general review; and to Dr. Ed Townsley and Mr. Peter Kysar (IDA) for their computational support. In addition, the author would also like to thank Mrs. Sharon Y. Wiley for her outstanding job of technical typing.

CONVERSION TABLE

Conversion factors for U.S. customary to metric (SI) units of measurement

To Convert From	To	Multiply
angstrom	meters (m)	1.000 000 X E–10
atmosphere (normal)	kilo pascal (kPa)	1.013 25 X E+2
bar	kilo pascal (kPa)	1.000 000 X E+2
barn	meter^2 (m^2)	1.000 000 X E–28
British Thermal unit (thermochemical)	joule (J)	1.054 350 X E+3
calorie (thermochemical)	joule (J)	4.184 000
cal (thermochemical)/cm^2	mega joule/m^2(MJ/m^2)	4.184 000 X E–2
curie	giga becquerel (GBq)*	3.700 000 X E+1
degree (angle)	radian (rad)	1.745 329 X E–2
degree Fahrenheit	degree kelvin (K)	$t_K=(t^\circ f + 459.67)/1.8$
electron volt	joule (J)	1.602 19 X E–19
erg	joule (J)	1.000 000 X E–7
erg/second	watt (W)	1.000 000 X E–7
foot	meter (m)	3.048 000 X E–1
foot–pound–force	joule (J)	1.355 818
gallon (U.S. liquid)	meter^3 (m^3)	3.785 412 X E–3
inch	meter (m)	2.540 000 X E–2
jerk	joule (J)	1.000 000 X E+9
joule/kilogram (J/Kg) (radiation dose absorbed)	Gray (Gy)	1.000 000
kilotons	terajoules	4.183
kip (1000 lbf)	newton (N)	4.448 222 X E+3
kip/inch^2 (ksi)	kilo pascal (kPa)	6.894 757 X E+3
ktap	newton–second/m^2 (N–s/m^2)	1.000 000 X E+2
micron	meter (m)	1.000 000 X E–6
mil	meter (m)	2.540 000 X E–5
mile (international)	meter (m)	1.609 344 X E+3
ounce	kilogram (kg)	2.834 952 X E–2
pound–force (lbf avoirdupois)	newton (N)	4.448 222
pound–force inch	newton–meter (N·m)	1.129 848 X E–1
pound–force/inch	newton/meter (N/m)	1.751 268 X E+2
pound–force/foot^2	kilo pascal (kPa)	4.788 026 X E–2
pound–force/inch^2 (psi)	kilo pascal (kPa)	6.894 757
pound–mass (lbm avoirdupois)	kilogram (kg)	4.535 924 X E–1
pound–mass–foot^2 (moment of inertia)	kilogram–meter^2 (kg·m^2)	4.214 011 X E–2
pound–mass/foot^3	kilogram/meter^3 (kg/m^3)	1.601 846 X E+1
rad (radiation dose absorbed)	Gray (Gy)**	1.000 000 X E–2
roentgen	coulomb/kilogram (C/kg)	2.579 760 X E–4
shake	second (s)	1.000 000 X E–8
slug	kilogram (kg)	1.459 390 X E+1
torr (mm Hg, 0°C)	kilo pascal (kPa)	1.333 22 X E–1

*The becquerel (Bq) is the SI unit of radioactivity; Bp = 1 event/s.

**The Gray (Gy) is the SI unit of absorbed radiation.

TABLE OF CONTENTS

FIGURES

SECTION 1
INTRODUCTION

This paper is part of an IDA Task about the "Characterization of Data and Utilization of Advanced Technologies for Predicting the Atmospheric Transport of Effluents from the Kuwaiti Oil Field Fires," being performed for the Defense Nuclear Agency (DNA). The Kuwaiti Oil Fires (KOF) of 1991 provided an opportunity for DNA to address some key questions about the atmospheric transport of particles that are relevant to the prediction of late-time dust and smoke cloud motion. During the fires, much data were collected by numerous U.S. and foreign scientific agencies, and now the critical issue is to assemble and organize a consistent set of measurements that can be evaluated against computer codes to predict small particle transport. These computer codes are required for the prediction of long-range transport of nuclear dust clouds and for the prediction of smoke plumes from large oil, industrial, or urban fires that might affect electro-optical sensor performance.

The KOF included features that were common with large forest fires, but the KOF also had other characteristics that made them unique. Bauer (Ref. 1) has provided an initial assessment of the characterization of the KOF in relation to various kinds of large fires and has identified certain key aspects that should be studied further. However, the reviewers of his document pointed out that when various long-range transport codes were exercised on KOF-like problems, the agreement was often not very good. This raises the following questions: Are the mathematical and physical models of the codes unsatisfactory? Are they being applied in situations for which they are not intended?

A key requirement for predicting particle transport is the necessity to follow the motion of some "tracer" particles (Lagrangian viewpoint). To be good tracers, the particles must remain physically and chemically inert during the transport process. This condition of physical and chemical invariance can be termed a "frozen" or "aged" state and applies to those particles sufficiently far away from the sources of the plume. Some of the processes that should be evaluated to ensure that transport calculations for the frozen state are performed properly include condensation and evaporation, accretion of water vapor or other species, combustion and other chemical reactions, Brownian coagulation, coagulation

in laminar shear flow, gravitational coagulation, turbulent shear coagulation, and turbulent inertial coagulation. Baumgardner (Ref. 2) has also suggested that turbulent mixing may have an effect on aerosol growth under certain circumstances. However, since all of these processes are most active during the initial stages of mass injection into the atmosphere and simple transport codes cannot be applied to a very young plume in which the tracer particles are not yet "aged," it is important to establish a minimum range to which a transport code can be applied for particles whose mass no longer changes with distance traveled.

In this paper, we make an initial assessment of the effects of turbulent shear coagulation and turbulent inertial coagulation on aerosol growth in the KOF. The results from this analysis may be useful in defining the "aged" regions that are applicable for particle transport analysis. Specific reasons for evaluating these turbulent coagulation processes in the KOF are as follows:

- Initial reported aerosol particle/mass densities are extremely high, leading to large coagulation growth rates.
- In the Canadian fire of 1950, turbulent coagulation was an important consideration (see Sections 2 and 3).
- Mass ejection is comparable to or exceeds that of large forest fires.
- There is a paucity of experimental data on turbulent coagulation in the atmosphere, and it may be necessary to have a means of interpreting certain KOF experimental data in this light.
- It is important to understand the dependence of turbulent coagulation on wind-speed (as it relates to transport time), turbulent kinetic energy dissipation rate per unit mass, aerosol density and size distribution, and atmospheric diffusion.
- The analytic representation of collection kernels for existing turbulent coagulation theories is based on spherical particles. While this may not be valid for KOF, it is necessary to have a simple way of estimating the changes in coagulation dynamics as a function of aerosol shape.

For mathematical simplicity, nearly all analyses involving the transport of particles from large fires have assumed that these particles have a spherical shape. Since a sphere has the smallest surface-to-volume (mass) ratio, these models usually place a lower bound on the reaction rate per mass unit . However, unlike a forest fire, in which roughly half of the condensed smoke particles are liquid and can be described a spheres, an oil fire presents a particular problem since most of the pure soot particles are long strands of solid carbon or more complex molecules and cannot really be described as spheres.

Evans et al. (Ref. 3) have examined the particle size and shape distribution for oil fires without interference from brine, water, nebulized tar, or dusty ambient aerosols and have shown that these smoke particles are an agglomeration of individual spherules that exhibit a strand-like behavior. A sample of their results is shown in Figure 1-1, which indicates that large numbers of strand-like particles may have existed in the many plumes from the KOF. This particle configuration would have an important effect on the time scale for kinetic processes and chemical reactions.

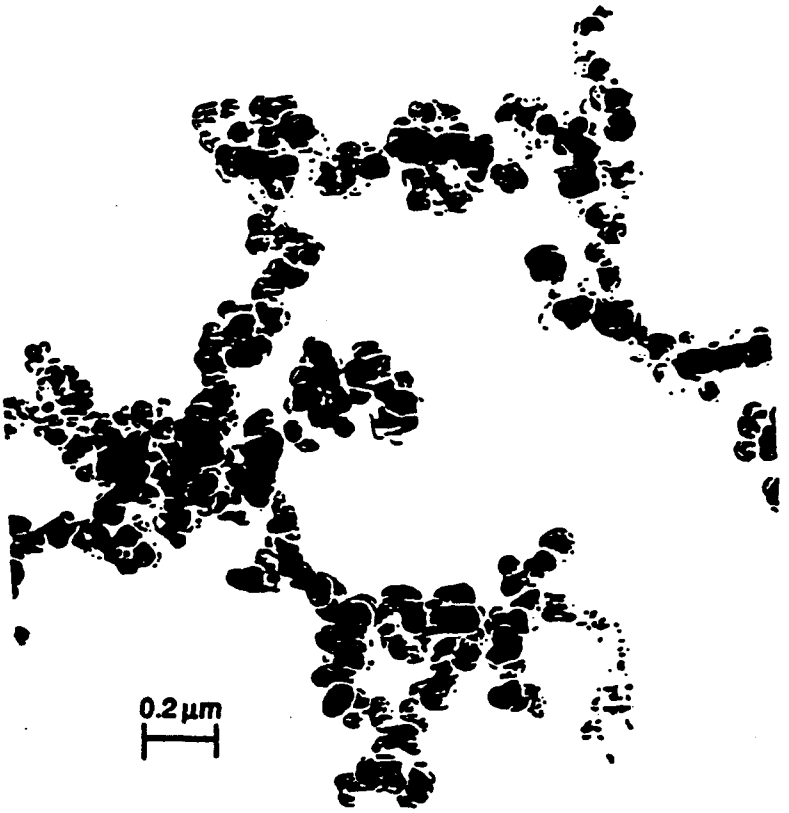

Figure 1-1. Electron micrograph of a smoke particle from a 1.0 m diameter murban crude oil fire (Source: Ref. 3).

In recent years, more attention has been paid to the fractal description of the irregular structures shown in Figure 1-1 and on the effects of such irregularities on free molecular agglomeration (Ref. 4). However, for the purposes of this study, we will assume a spherical shape for all particles and apply a correction factor when more accurate analysis becomes available.

It should be emphasized that the selection of the turbulent coagulation processes as the first of the aging processes to be considered does not imply that the others have been deemed to be less important. Indeed, we plan to address the other aging processes in a subsequent publication in which we will make use of the mathematical formalism established in this study.

In Section 2 of this paper, we evaluate the dependence of turbulent shear coagulation and turbulent inertial coagulation on aerosol concentration and mass density, size distribution, and turbulence parameters. These considerations are then applied to the KOF in Section 3, in which the effects of windspeed, atmosphere turbulence, and aerosol emission rate are taken into account. Concluding remarks are rendered in Section 4.

SECTION 2
TURBULENT COAGULATION PROCESSES

Because the conditions of the KOF have not been encountered before, we have a limited data base for predicting the spatial regions and conditions for which turbulent coagulation may be important. It is also unlikely that simple transport codes will be valid for this type of assessment. One of the reasons for examining the significance of turbulent coagulation in the KOF is that the initial reported particle concentrations are extremely high. For example, Hobbs and Radke (Ref. 5) report particle concentrations frequently exceeding 10^5 cm^{-3} within a few kilometers from the fires and mass concentrations of the composite plume ~840 μg m^{-3} at 20 km downwind for particles <3.5 μm in diameter. Johnson et al. (Ref. 6) report mass densities between 500-1000 μg m^{-3} at distances greater than 200 km. These observations suggest that coagulation processes could be important over a significant spatial region. In this section and in Section 3, we examine this conjecture.

Recently, Porch (Ref. 7) has examined the impact of turbulent coagulation on the size distribution of aerosols produced by large fires in an attempt to understand the phenomenon of Blue Moons. Porch used models where initial mass concentrations for spherical smoke particles with radii less than 1 μm ranged from 5×10^{-9} to 5×10^{-8} g cm^{-3} (or equivalently 5000 to 50,000 μg m^{-3}). These estimates appear to apply over the fire itself, represented in Porch's model by a diameter of 400 km. In an earlier study, Porch, Penner, and Gillette (Ref. 8) conducted a numerical study of the effects of super-μm particles on the coagulation loss of submicron particles. The results of these studies have shown that for particles with radii less than 0.1 μm Brownian coagulation is more rapid than turbulent coagulation, while the latter mechanism generally dominates for particle sizes of a few microns (Ref. 9).

The basic model for turbulent coagulation was developed by Saffman and Turner (Ref. 10), who identified the two distinct coagulation mechanisms: turbulent shear coagulation and turbulent inertial coagulation. Pruppacher and Klett (Ref. 9) have succinctly summarized the salient features of turbulent coagulation. The first significant feature is that turbulent coagulation applies to those aerosols of radius $r << \lambda_k$ where λ_k is the "Kolmogorov microscale length" (Refs. 9, 10). As shown in Table 2-1, this is

satisfied for the conditions of KOF, in which virtually all of the aerosol particles have dimensions less than the indicated values of λ_k.

Table 2-I. Kolmogorov microscales as a function of energy dissipation rate, ε.

ε ($cm^2\ s^{-3}$)	λ_k (cm)	τ_k (s)	Comment
5	1.8×10^{-1}	1.9×10^{-1}	Applicable to stratiform clouds where there is small mean velocity (Ref. 10)
100	8.4×10^{-2}	4.1×10^{-2}	Cloudy air (Ref. 9)
1000	4.8×10^{-2}	1.3×10^{-2}	Relevant for conditions in turbulent cumulus clouds (Ref. 10)
2000	4.0×10^{-2}	9.3×10^{-3}	Relevant to early stages of the plume in large fires (Ref. 7)
8000	2.8×10^{-2}	4.6×10^{-3}	Exceptional case of turbulent shear in high turbulence (Ref. 8)

Coagulation results from the velocity motion between particles. One method of achieving relative motion is through significant small-scale velocity gradients in turbulent flow. For the length scale of velocity gradients that are smaller than λ_k, the coagulation process is similar to that of the laminar shear flow case considered by Smoluchowski and described in Pruppacher and Klett (Ref. 9). If m_1, m_2 are the masses of the coagulating particles, and r_1 and r_2 are their respective radii, and ρ is the material intrinsic density (assumed the same for both/all particles), and

$$m = \frac{4}{3}\pi \rho r^3 \quad , \tag{2.1}$$

then the collection kernel for *turbulent shear coagulation* is given by (Refs. 9, 10):

$$K_S(m_1, m_2) = 1.3(r_1 + r_2)^3 \tau_k^{-1} \text{ cm}^3 \text{ s}^{-1} \quad , \tag{2.2}$$

where τ_k is the "Kolmogorov time scale" (Refs. 9, 10).

Another method for producing a relative particle velocity is due to local turbulent accelerations. Particles of different mass respond differently to these accelerations by having different viscous relaxation times associated with velocity equilibration. This leads to the following expression for the collection kernel for *turbulent inertial coagulation:*

$$K_I(m_1, m_2) = \frac{2\pi}{9} \frac{\rho}{\rho_A} (r_1 + r_2)^2 \, |r_1^2 - r_2^2| \, \tau_k^{-1} \lambda_k^{-1} \ \text{cm}^3 \, \text{s}^{-1} \ . \qquad (2.3)$$

In this equation, ρ_A is the air mass density, and λ_k and τ_k are the Kolmogorov microscales for length and time, which are given by

$$\lambda_k = \left(\frac{\nu^3}{\varepsilon}\right)^{1/4} \text{cm} \qquad (2.4)$$

$$\tau_k = \left(\frac{\nu}{\varepsilon}\right)^{1/2} \text{s} \ , \qquad (2.5)$$

where ε is the dissipation rate of kinetic energy per unit mass ($\text{cm}^2\ \text{s}^{-3}$) and ν is the kinetic viscosity of air ($\text{cm}^2\ \text{s}^{-1}$). For the altitude range used in our study, we take the U.S. Standard Atmosphere values of $\rho_A = 10^{-3}\ \text{g cm}^{-3}$ and $\nu = 0.172\ \text{cm}^2\ \text{s}^{-1}$.

As observed in Equations (2.4) and (2.5), the dissipation rate is a key parameter. Table 2-1 gives values of λ_k and τ_k for selected values of ε. Examination of this table shows that values of ε ranging from 2000 to 8000 $\text{cm}^2\ \text{s}^{-3}$ are being considered in this study.

Some of the important mathematical and physical characteristics of the coagulation process can be presented best by considering the time behavior of the aerosol distribution in a spatially uniform medium. We let f(m, t) dm be the number of particles per unit volume lying in the mass range between m and m + dm, where f(m, t) is defined as the mass density function (MDF). Using $K(m_1, m_2)$ as the general description for either of the collection kernels [Equation (2.2) or (2.3)] gives the following equation for the time evolution of f(m, t):

$$\frac{\partial f}{\partial t} = \frac{1}{2} \int_{m_1} \int_{m_2} K(m_1, m_2)\, f(m_1)\, f(m_2)\, \delta(m - m_1 - m_2)\, dm_1\, dm_2$$

$$- f(m) \int_{m_2} K(m, m_2)\, f(m_2)\, dm_2 \ . \qquad (2.6)$$

The first term in Equation (2.6) is the growth term. The "1/2" appearing in front of the integral is due to the fact that there is a reduction of one particle when two particles coagulate. Inclusion of the Delta function $\delta(m - m_1 - m_2)$ selects from all collisions only those in which the mass, m, equals $m_1 + m_2$. It is possible to integrate the growth term

over either of the dummy variables m_1 or m_2 in Equation (2.6) and simplify the integral to the more familiar form (Ref. 7),

$$\frac{1}{2}\int_{m_1}\int_{m_2} K(m_1, m_2)\, f(m_1)\, f(m_2)\, \delta(m - m_1 - m_2)\, dm_1\, dm_2$$

$$= \frac{1}{2}\int_0^m K(m - m_2, m_2)\, f(m - m_2)\, f(m_2)\, dm_2 \quad , \tag{2.7}$$

which is obtained by integration over m_1. The second term in Equation (2.6) is the loss due to coagulation and is the integration over all possible events.

A further condition that is not explicitly represented in the expressions for K_S and K_I is the existence of an efficiency factor associated with coagulation. For usual turbulent clouds, Saffman and Turner (Ref. 10) suggest that the probability of coagulation may be close to unity when particles are about the same size but diminishes rapidly for particles of very different size. The coagulation efficiency of the KOF is not clear since the particles are not water droplets. The issue of collection efficiency is difficult to address in this preliminary assessment, particularly since many of the KOF particles may not be spherical. Hence, for the present we will not include this consideration in our model.

For this study, we assume an efficiency of unity for all colliding particles. We also assume that all particles are spherical since the collection kernels have only been modeled for this case. A preliminary estimate of the collection efficiency for nonspherical particles suggests that it would be greater than that for spherical particles of the same mass.

A more precise evaluation of the collection kernel(s) could perhaps be obtained by extending the Saffman and Turner (Ref. 10) analysis to more realistic shapes. However, until such an analysis becomes available, we will use the spherical models. At the end of the analysis, it is possible to apply a correction factor to account for enhancement in the coagulation process. Although we do not explicitly include this correction factor in this analysis,[1] it is used in the discussion of results.

---

1 Actually, the combined effect of collisions and the probability of particles sticking together after the collision are both important. On one hand, the use of spherical aerosols appears to underestimate the collection kernel; however, this is counterbalanced in our model by assuming that the particles stick together in every collision. If estimates of the relevance of turbulent coagulation in KOF turn out to be important in long-range transport prediction, it may be necessary to examine these issues further.

Using Equation (2.6), we can make certain observations about the coagulation dynamics to obtain an estimate of the relevant time constants as a function of particle density and dissipation rate. We first note that the mass density, M, where

$$M = \int mf(m)\, dm \ , \tag{2.8}$$

remains invariant. We can demonstrate this by multiplying both sides of Equation (2.6) by m and then integrating over all mass space. Thus, we have

$$\frac{\partial M}{\partial t} = \frac{1}{2} \int_{m_1} \int_{m_2} K(m_1, m_2)\,(m_1+m_2)\, dm_1\, dm_2$$

$$- \int_{m_1} \int_{m_2} mK(m, m_2)\, dm\, dm_2 \ . \tag{2.9}$$

The first term in Equation (2.9) was obtained through the integration $\int m\, \delta(m - m_1 - m_2)\, dm$. Since $K(m_1, m_2)$ and $K(m, m_2)$ are symmetric kernels, the right-hand side of Equation (2.9) equals zero and thus

$$\frac{\partial M}{\partial t} = 0 \tag{2.10}$$

as expected.

The total number of particles per cm^3 is defined as

$$N(t) = \int f(m,t)\, dm \tag{2.11}$$

and is determined from Equation (2.6) by integration over mass space. We obtain

$$\frac{\partial N}{\partial t} = \frac{1}{2} \int_{m_1} \int_{m_2} K(m_1, m_2)\, f(m_1)\, f(m_2)\, dm_1\, dm_2$$

$$- \int_{m_1} \int_{m_2} K(m_1, m_2)\, f(m_1)\, f(m_2)\, dm_1\, dm_2$$

$$= -\frac{1}{2} \int_{m_1} \int_{m_2} K(m_1, m_2)\, f(m_1)\, f(m_2)\, dm_1\, dm_2 \ . \tag{2.12}$$

Improved insight into the kinetics of coagulation is gained by introducing a normalized mass density function (NMDF), $\phi(m, t)$, through the equation

$$f(m, t) = N(t)\,\phi(m, t) \quad . \tag{2.13}$$

From Equation (2.11), we deduce the required normalization condition

$$\int \phi(m, t)\, dm = 1 \quad . \tag{2.14}$$

By introducing $\phi(m, t)$, we can cast the analysis in terms of those issues that are attributed solely to the total aerosol concentration, N(t), and those issues that are due to the distribution in mass as given by $\phi(m, t)$. Substituting Equation (2.13) into Equation (2.12) gives

$$\frac{\partial N}{\partial t} = -\frac{1}{2} N^2 \eta(t) \quad , \tag{2.15}$$

where

$$\eta(t) = \int_{m_1} \int_{m_2} K(m_1, m_2)\, \phi(m_1, t)\, \phi(m_2, t)\, dm_1 dm_2 \quad . \tag{2.16}$$

For the special situation in which the collection kernel is assumed to be mass-independent, that is, $K(m_1, m_2) = K_o$, a constant, the result is

$$\frac{\partial N}{\partial t} = -\frac{1}{2} N^2 K_o \quad . \tag{2.17}$$

The solution to Equation (2.17) is

$$N(t) = \frac{N_i}{1 + (N_i K_o t)/2} \quad , \tag{2.18}$$

where N_i is the initial concentration.

We will now make an estimate of $\eta(t)$ using the analytical forms of $K_S(m_1, m_2)$ and $K_I(m_1, m_2)$ from Equations (2.2) and (2.3) in combination with certain experimental results of Radke et al. (Ref. 11) and as reported by Porch (Ref. 7), which lead to an assessment of $\phi(m, t)$. Because K_S and K_I are easier to work with in terms of aerosol radius instead of mass, it is convenient in computing $\eta(t)$ to express the mass distribution in terms of the aerosol radius distribution. Introducing a normalized particle radius function (NPRF), g(r, t), and applying the transformation law for probability frequency functions gives

$$\phi(m)\, dm = g(r)\, dr \quad , \tag{2.19}$$

where m and r are related by Equation (2.1). As seen in Equation (2.19), a knowledge of either ϕ or g determines the other by differentiating Equation (2.1).

For the turbulent shear coagulation model, the expansion of $(r_1 + r_2)^3$ in Equation (2.2) gives

$$K_S = (1.3)\,\tau_k^{-1}\left(r_1 + r_2\right)^3$$

$$= (1.3)\tau_k^{-1}\left(r_1^3 + 3r_1^2 r_2 + 3r_1 r_2^2 + r_2^3\right) \quad . \tag{2.20}$$

Substituting Equation (2.20) into Equation (2.16) and using the property that K_S is symmetric in r_1 and r_2 yields

$$\eta_S(t) = 1.3\tau_k^{-1}\left(2\overline{r^3} + 6\overline{r^2}\,\bar{r}\right) \quad .$$

$$= 2.6\tau_k^{-1}\,\overline{r^3}\left(1 + 3\overline{r^2}\,\bar{r}/\overline{r^3}\right) \quad , \tag{2.21}$$

where

$$\overline{r^3} = \int r^3\, g(r, t)\, dr = \frac{3}{4\pi}\,\rho^{-1}\int m\,\phi(m, t)\, dm = \frac{3}{4\pi}\rho^{-1}\,\overline{m} \quad , \tag{2.22}$$

$$\overline{r^2} = \int r\, g(r, t)\, dr \quad , \tag{2.23}$$

$$\bar{r} = \int r\, g(r, t)\, dr \quad , \tag{2.24}$$

and

$$\overline{m} = \int m\,\phi(m, t)\, dm \quad . \tag{2.25}$$

$\overline{m}$ is the average mass of all particles as can be seen from the definition

$$\overline{m} = \frac{\int m\, f(m, t)\, dm}{N(t)} = \frac{M}{N(t)} = \int m\,\phi(m, t)\, dm \quad . \tag{2.26}$$

Let us temporarily assume that $3\,\overline{r^2}\,\bar{r}/\overline{r^3}$ is much less than unity [we will partially substantiate this assumption using Radke's data (Ref. 11)]. Then $\eta_S(t)$ is approximately given by

$$\eta_S(t) = 2.6\,\tau_k^{-1}\,\frac{3}{4\pi}\,\rho^{-1}\,\overline{m} \quad . \tag{2.27}$$

Substituting Equation (2.27) into Equation (2.15) gives

$$\frac{\partial N}{\partial t} = -\frac{0.31}{\tau_k \rho}\,(N\,\overline{m})\,N \quad . \tag{2.28}$$

On the other hand, since the total mass density, $M = N\overline{m}$, remains constant during the coagulation process, turbulent shear coagulation can be approximated by the simple equation

$$\frac{\partial N}{\partial t} = -\frac{N}{T_S} \quad , \tag{2.29}$$

where

$$T_S = \frac{3.2\,\tau_k\,\rho}{M} \quad . \tag{2.30}$$

The smallest values of T_S correspond to small values of τ_k (high levels of turbulence) and large values of M. Using $M = 5 \times 10^{-8}$ g cm^{-3}, $\rho = 1.0$ g cm^{-3}, and $\tau_k = 4.6 \times 10^{-3}$ s (corresponding to $\varepsilon = 8000$ cm^2 s^{-3}) gives an e-folding time of

$$T_S = 2.9 \times 10^5 \text{ s} = 81 \text{ hr} \quad , \tag{2.31}$$

which appears quite long when compared to the time scales of interest in the KOF.

Let us now return to evaluating the term

$$3\,\overline{r^2}\,\bar{r}/\overline{r^3} = \Delta \quad , \tag{2.32}$$

which first appeared in Equation (2.21) and was subsequently neglected in the derivation of Equation (2.28). Δ may be considered a "correction factor" and in the approximation of Equation (2.27) has been neglected. However, as shown in Equations (2.22) to (2.24), each of the entities, $\bar{r}$, $\overline{r^2}$, and $\overline{r^3}$, involved in the computation of Δ is time dependent since g(r, t) changes with time. Essentially, $\Delta(t)$ cannot be determined exactly without solving the problem exactly. However, it is interesting to explore the conditions under which Δ is negligible and under which it is greater than unity, the latter condition requiring modification of Equation (2.28).

An estimate of Δ can be obtained using measurements of what Radke (Ref. 11) calls the *Number Size Distribution*. In his notation, this quantity is labeled "dN/dR" (see

Figure 2-1) and is defined as the number of particles per unit radius per unit volume. In our formalism, we express this quantity as N g(r) and have

$$\frac{dN}{dR} = N\, g(r) \quad . \tag{2.33}$$

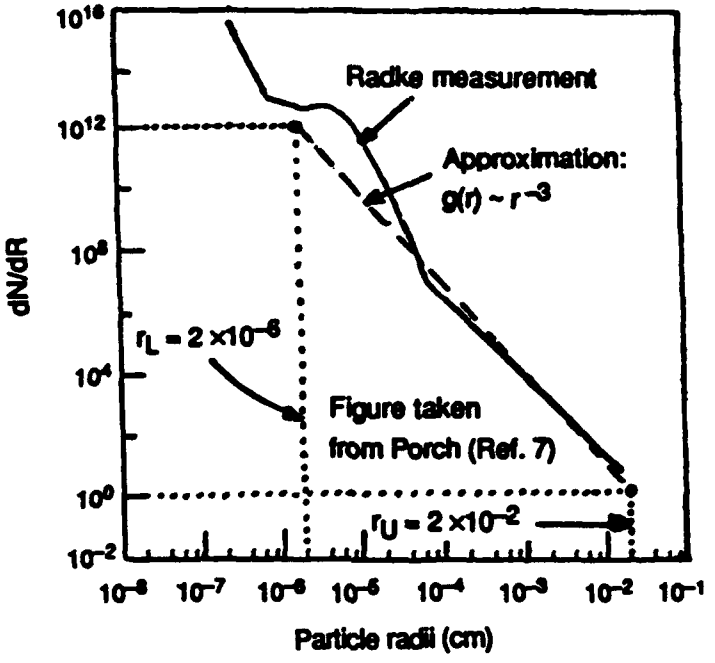

Figure 2-1. Number size distribution of particles observed in a forest slash fire (Source: Ref. 11).

The solid line in Figure 2-1 is dN/dR at the beginning phases of a forest slash fire. The dashed line in this figure is an approximation of dN/dR, which is necessary for the approximate analytical assessment used in our study. The approximation of Figure 2-1 applies in the radius range extending from a lower limit of 2×10^{-6} cm to an upper limit of 2×10^{-2} cm and describes a distribution that varies as r^{-3}.

We should emphasize that the *Number Size Distribution* of Figure 2-1 is taken at an instant of time. However, during the coagulation process, g(r, t) will change with time as the size distribution shifts to larger particles (Ref. 7). In addition, the g(r) of this figure applies to a forest slash fire and would likely be different from the g(r) of the KOF. Nevertheless, the use of g(r) from Figure 2-1 provides a mathematical basis for examining

the importance of the radial shape function on coagulation dynamics, and, therefore, we assume that g(r) for the KOF is similar to the result for Figure 2-1.

The sensitivity of the results to the analytic representation of the aerosol distribution can be explained by proposing that g(r) for the KOF varies as r^{-s} between a lower limit, r_L, and an upper limit, r_U. This form of the approximation for g(r) is chosen because of its mathematical simplicity and because it is representative of aerosol size distributions found in nature before the onset of significant aging caused by coagulation. For this case, we have

$$g(r) = A\, r^{-s} \quad , \tag{2.34}$$

where A is the normalization constant determined from the requirement that $\int_0^\infty g(r)\, dr = 1$. Applying the normalization condition gives

$$A = (s-1)\, r_L^{s-1} \left(1 - (r_L / r_U)^{s-1}\right)^{-1} \quad . \tag{2.35}$$

From Figure 2-1, we have $r_L = 2 \times 10^{-6}$ cm and $r_U = 2 \times 10^{-2}$ cm. The ratio r_L/r_U equals 10^{-4} and is therefore negligible. In this case, we have the approximation

$$A = (s-1)\, r_L^{s-1} \quad . \tag{2.36}$$

For expediency, we also assume that Equation (2.36) applies for the KOF, although this assumption can readily be modified using actual data. Lastly, it should be stated that Equation (2.34) implies a time-invariant size distribution, which is clearly not the case. Despite this limitation, Equation (2.34) provides a basis for understanding the important features of the size distribution in regard to the coagulation process.

Equation (2.34) readily furnishes the expression for the nth moment:

$$\overline{r^n} = \int_{r_L}^{r_U} r^n g(r) dr = \left(\frac{r_L^n}{n+1-s}\right)\left(Q^{n+1-s} - 1\right) \quad , \tag{2.37}$$

where

$$Q = \left(r_U / r_L\right) \quad . \tag{2.38}$$

The moments $\bar{r}$, $\overline{r^2}$, and $\overline{r^3}$ are readily computed from Equation (2.37). Inserting the resulting expressions into Equation (2.32) gives

$$\Delta = \frac{3\,(4-s)}{(2-s)\,(3-s)} \frac{\left(Q^{2-s}-1\right)\left(Q^{3-s}-1\right)}{\left(Q^{4-s}-1\right)} \quad . \tag{2.39}$$

We now examine the dependence of Δ on s in the range where $Q >> 1$. These results are shown in Table 2-2 and are obtained by taking the limit of Equation (2.39) for $Q = r_U/r_L >> 1$. This is the range of interest for forest fires but also appears to be the range of interest for KOF, based on preliminary data obtained from Baumgardner (Ref. 12). It should be noted that the expressions in Table 2-2 cannot be applied at the integer values of $s = 2, 3, 4$. In order to compute Δ at these values, the limiting form of Equation (2.39) at $s = 2, 3, 4$, respectively, must be taken using L'Hopital's rule. Figure 2-2 provides a broader perspective of the dependence of Δ on s and Q.

Table 2-2. Dependence of Δ on s.

s	Δ
$1 < s < 2$	$\frac{3(4-s)}{(2-s)\,(3-s)} \left(\frac{r_U}{r_L}\right)^{1-s}$
$2 < s < 3$	$\frac{3(4-s)}{(s-2)\,(3-s)} \left(\frac{r_L}{r_U}\right)$
$3 < s < 4$	$\frac{3(4-s)}{(s-2)\,(s-3)} \left(\frac{r_L}{r_U}\right)^{4-s}$
$4 < s$	$\frac{3(s-4)}{(s-2)\,(s-3)}$

Examination of Table 2-2 shows that the correction factor Δ is negligible for $s > 2$ since $r_L/r_U << 1$. On the other hand, in the range $1 < s < 2$, the variation of Δ with r_U/r_L shows that the correction factor can be several orders of magnitude greater than unity. This is also indicated in Figure 2-2. Should g(r) vary as r^{-s} with $1 < s < 2$, the time constant, T_S, in Equation (2.30) could be reduced by several orders of magnitude, rendering turbulent shear coagulation a very important consideration since the effective time scale would be reduced to approximately 1 hour. It is important to note that significant coagulation effects involving time scales under 1 hour and for particles greater than 1 μm in

radius have been computed for the large Canadian forest fire of 1950 using Radke's results in Figure 2-1 (Ref. 7).

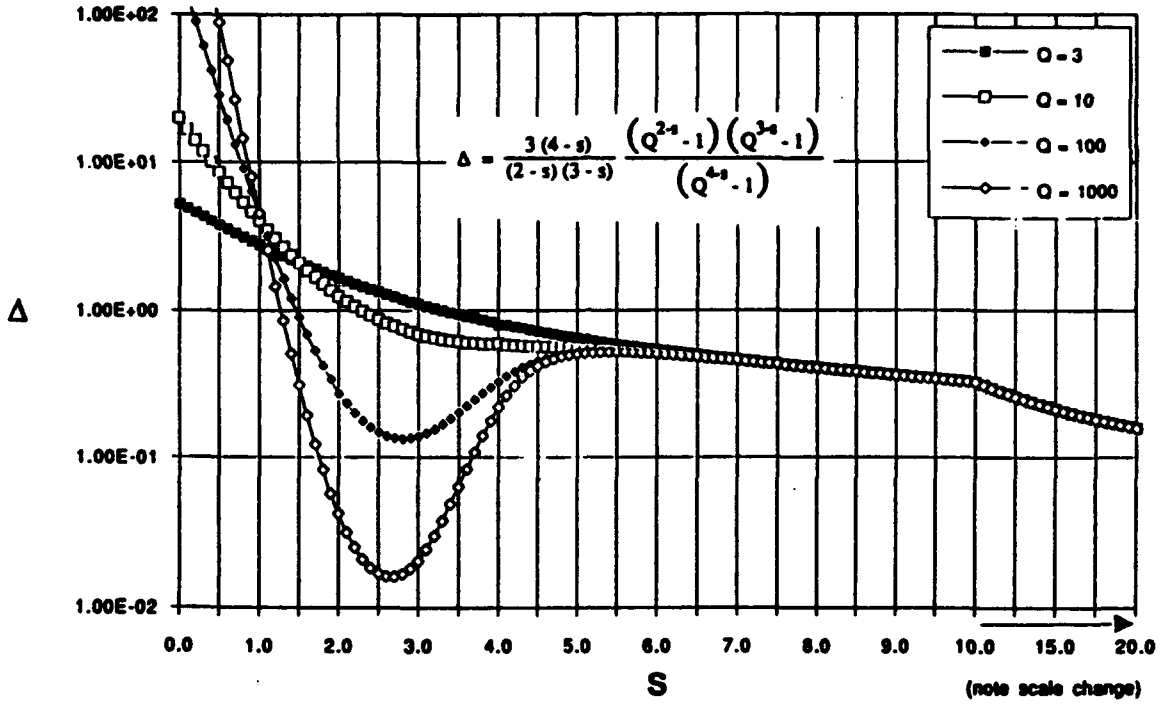

Figure 2-2. Δ as a function of s with Q as a parameter.

Up to this point, we have only considered the contribution from turbulent shear coagulation through use of the collection kernel given by Equation (2.2). We now consider the contribution from turbulent inertial coagulation in Equation (2.3). Using Equation (2.16), the corresponding parameter, η_I, is given by

$$\eta_I = B \int_{r_1} \int_{r_2} (r_1 + r_2)^2 \, |r_1^2 - r_2^2| \, g(r_1) \, g(r_2) \, dr_1 \, dr_2 \quad , \tag{2.40}$$

where

$$B = \frac{2\pi}{9} \frac{\rho}{\rho_A} \frac{1}{\tau_k \lambda_k} \quad . \tag{2.41}$$

In contrast to the case for turbulent shear coagulation, the double integration over r_1, r_2 is not separable due to the nonanalytic function $|r_1^2 - r_2^2|$. However, it is possible to obtain a lower bound on η_T in the following way. Consider the integrals I_1 and I_2, where

$$I_1 = \int_{r_1} \int_{r_2} (r_1 + r_2)^2 |r_1^2 - r_2^2| g(r_1)\, g(r_2)\, dr_1\, dr_2 \tag{2.42}$$

and

$$I_2 = \int_{r_1} \int_{r_2} (r_1 + r_2)^2 (r_1 - r_2)^2\, g(r_1)\, g(r_2)\, dr_1\, dr_2 \ . \tag{2.43}$$

I_1 appears in Equation (2.40). I_2 is similar and has the essential property required of I_1, namely, ensuring that no contribution comes from the domain where $r_1 \approx r_2$.

We now show that $I_1 > I_2$. Let

$$a = |r_1^2 - r_2^2| = (r_1 + r_2)|r_1 - r_2| \tag{2.44}$$

and

$$b = (r_1 - r_2)^2 = (r_1 - r_2)(r_1 - r_2) \tag{2.45}$$

and consider the difference

$$\begin{aligned} \Omega &= a^2 - b^2 \\ &= (r_1 + r_2)^2 (r_1 - r_2)^2 - (r_1 - r_2)^4 = (r_1 - r_2)^2\, 4 r_1 r_2 \geq 0 \ . \end{aligned} \tag{2.46}$$

Since a, b are > 0, and $a^2 \geq b^2$, we conclude that $a \geq b$. Therefore,

$$I_1 > I_2 \ . \tag{2.47}$$

A lower bound on η_I, defined as η_I^*, is thus given by

$$\eta_I^* = B\, I_2 \ . \tag{2.48}$$

Use of η_I^* provides a minimum rate of coagulation by inertial turbulence. The integration of I_2 yields

$$I_2 = 2\left(\overline{r^4} - \overline{r^2}\,\overline{r^2}\right) = 2\overline{r^4}\left(1 - \frac{\left(\overline{r^2}\right)^2}{\overline{r^4}}\right) \tag{2.49}$$

The ratio $\theta = \left(\overline{r^2}\right)^2 / \overline{r^4}$ is deduced from Equation (2.37) to yield

$$\theta = \frac{\left(\overline{r^2}\right)^2}{\overline{r^4}} = \frac{5-s}{(3-s)^2}\,\frac{\left(Q^{3-s}-1\right)^2}{\left(Q^{5-s}-1\right)} \tag{2.50}$$

Table 2-3 shows the dependence of θ on s for the range of interest $r_U/r_L = Q >> 1$, and Figure 2-3 shows θ as a function of s with Q as a parameter. It should be noted that the expressions in Table 2-3 cannot be applied at the integer values of s = 3, 5. At these values of s, θ must be computed from Equation (2.50) using L'Hopital's rule.

Table 2-3. Dependence of θ on s.

s	θ
$1 < s < 3$	$\frac{5-s}{(3-s)^2}\left(\frac{r_L}{r_U}\right)^{s-1}$
$3 < s < 5$	$\frac{5-s}{(s-3)^2}\left(\frac{r_L}{r_U}\right)^{5-s}$
$5 < s$	$\frac{s-5}{(s-3)^2}$

Since the anticipated range of interest is from s = 3 to s = 5 and for $Q >> 1$, we conclude from both Table 2-3 and Figure 2-3 that θ can be neglected in comparison to unity and thus use the approximation

$$= 2\overline{r^4} = \frac{2r_L^4}{(5\text{-}s)}\left(Q^{5-s}-1\right) . \tag{2.51}$$

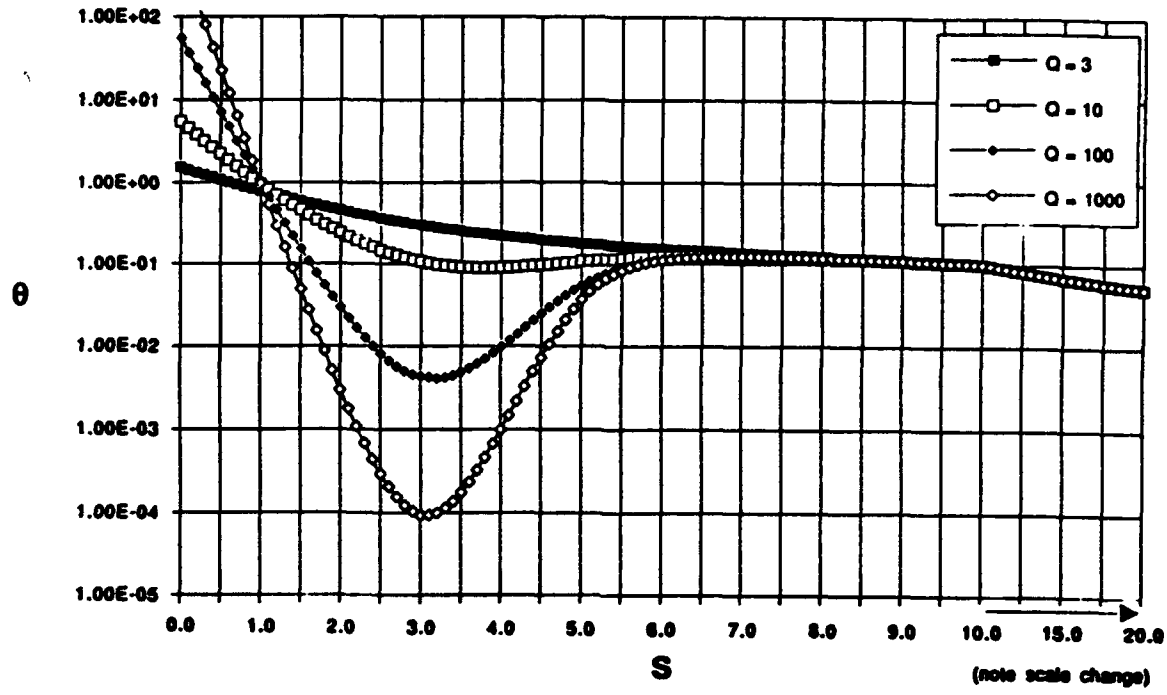

Figure 2-3. θ as a function of s with Q as a parameter.

Using the results from Table 2-2 and neglecting the contribution from Δ for $s > 2$ provide a comparison of the relative contribution for shear and inertial coagulation. For $s > 2$, we have

$$\eta_S = 2.6\,\tau_k^{-1}\,\overline{r^3} \tag{2.52}$$

and

$$\eta_I^* = \frac{4\pi}{9}\,\frac{\rho}{\rho_A}\,\tau_k^{-1}\,\lambda_k^{-1}\,\overline{r^4} \tag{2.53}$$

and the ratio η_I^*/η_S is given by

$$\frac{\eta_I^*}{\eta_S} = (0.54)\left(\frac{\rho}{\rho_A}\right)\left(\frac{4-s}{5-s}\right)\frac{r_L}{\lambda_k}\,\frac{\left(Q^{5-s}-1\right)}{\left(Q^{4-s}-1\right)} \tag{2.54}$$

In the subsequent calculations, we use $\rho = 1$ g cm^{-3} for the aerosol particles, and $\rho_A = 10^{-3}$ g cm^{-3}. There is dramatic variation of η_I^*/η_S as a function of s. This quantity

can vary over several orders of magnitude, depending on the ratio r_U/r_L (as long as $r_U/r_L >> 1$). For example, when $2 < s < 4$, Equation (2.54) reduces to

$$\frac{\eta_I^*}{\eta_S} = (540)\,\frac{(4-s)}{(5-s)}\,\frac{r_U}{\lambda_k} \quad , \tag{2.55}$$

while for $s > 5$ we have

$$\frac{\eta_I^*}{\eta_S} = (540)\left(\frac{s-4}{s-5}\right)\frac{r_L}{\lambda_k} \quad . \tag{2.56}$$

The ratio between Equations (2.55) and (2.56) is approximately given by r_U/r_L, which may range several orders of magnitude (e.g., $r_U/r_L = 10^4$ in Figure 2-1).

It is interesting to examine η_I^*/η_S in the range $2 < s < 4$ for a representative large value of dissipation rate. Using the value $\lambda_k = 4 \times 10^{-2}$ cm from Table 2-1, corresponding to $\varepsilon = 2000$, and $r_U = 2 \times 10^{-2}$ and the value $s = 3$ deduced from Figure 2-1 gives

$$\frac{\eta_I^*}{\eta_S} = \frac{(540)}{4} = 135 \quad . \tag{2.57}$$

If η_I^* were to be used in the formalism of Equations (2.28) to (2.30), the time constant would be T_I instead of T_S and would be given by

$$T_I = \frac{T_S}{135} = \frac{2.9 \times 10^5}{135} = 2.1 \times 10^3 \text{ s} = 35 \text{ min} \quad . \tag{2.58}$$

The results show that inertial coagulation is the dominant mechanism for particle frequency functions that contain a substantial fraction of particles greater than 1 μm. This conclusion is also consistent with the general observations made by Pruppacher and Klett (Ref. 9).

SECTION 3
APPLICATION TO KOF

The purpose of this section is to examine the geometric boundary(ies) of KOF where turbulent coagulation no longer contributes to the aging of aerosols. When combined with the results of other aerosol mass changing processes, this analysis will contribute to defining the overall spatial region(s) of KOF where aerosols no longer experience mass changing. These are the only regions where it is meaningful to compare the concentration prediction capability of current-generation particle transport codes (which do not include aging effects) to experimental results.

Figure 3-1 depicts the KOF plume behavior for turbulent coagulation considerations. This figure portrays three individual plumes merging into a superplume. The actual KOF aerosol problem is one in which the particle concentration of a superplume is forged by the merging of hundreds of individual plumes.

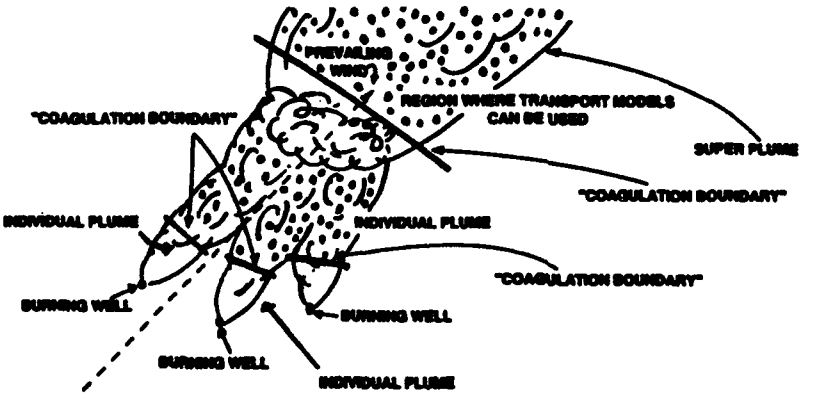

Figure 3-1. Geometric viewpoint for coagulation considerations.

In this figure, we hypothesize that there will be significant coagulation effects as the flames emerge from each individual well since the concentration/mass density will be extremely high. As the individual plumes spread, the concentrations will decrease by geometric dilution caused by atmospheric turbulence and coagulation. Ultimately, we

propose that the coagulation process becomes insignificant due to decreasing particle concentrations. The surfaces that define this transition are labeled "Coagulation Boundary." The shaded areas beyond these boundaries are the regions where coagulation is assumed to be insignificant.

Figure 3-1 suggests the possibility that the merging plumes may again produce conditions for coagulation; hence, another Coagulation Boundary is shown in the superplume. However, Sykes (Ref. 13) has questioned the possibility of a secondary coagulation boundary for the merged plumes on the grounds that this could not occur without some mechanism for concentrating particles locally. This issue will be resolved when detailed and reliable data are available from the field experiment.

The specific objective of this section is to develop a mathematical model for predicting the downwind aerosol density for either an individual fire or a merged plume and, from this model, to determine the Coagulation Boundaries shown in Figure 3-1. The analytical model is developed by combining the turbulent coagulation kinetics described in Section 2 with particle transport and incorporating advection and turbulent diffusion.

In Section 2, we showed that the aerosol concentration for a spatially uniform medium is given by

$$\frac{\partial N}{\partial t} = -\frac{1}{2} N^2 \eta(t) \quad , \tag{3.1}$$

where $\eta(t)$ can be written as

$$\eta(t) = \int_{r_1} \int_{r_2} K\left[m_1(r_1), m_2(r_2)\right] g(r_1, t)\, g(r_2, t)\, dr_1 dr_2 \quad . \tag{3.2}$$

Equation (3.2) is the same as Equation (2.16) but is now written in terms of the radius variables. Summarizing the results from Section 2, we have the following for *turbulent shear coagulation*:

$$\eta_S = 2.6\, \tau_k^{-1}\, \overline{r^3}\, (1 + \Delta) \quad , \tag{3.3}$$

where

$$\Delta = 3\overline{r^2}\, \bar{r} / \overline{r^3} \quad . \tag{3.4}$$

For *turbulent inertial coagulation*, we have

$$\eta_I^* = \frac{4\pi}{9} \frac{\rho}{\rho_A} \frac{\overline{r^4}}{\tau_k \lambda_k} (1 - \theta) \quad , \tag{3.5}$$

where

$$\theta = \left(\overline{r^2}\right)^2 / \overline{r^4} \quad . \tag{3.6}$$

It should be noted that Equation (3.3) is a restatement of Equation (2.21) and Equation (3.5) is a restatement of Equation (2.48) using the exact expression of I_2 of Equation (2.49) instead of neglecting θ.

As indicated in Equations (3.3) to (3.6), a knowledge of the first four moments of g(r, t), $\bar{r}$, $\overline{r^2}$, $\overline{r^3}$, and $\overline{r^4}$, precisely determines the time evolution of the aerosol density. It should be stressed that these quantities apply to any functional form of g(r, t). Thus, any measurements of aerosol properties that could furnish information regarding the first four moments would be sufficient to determine the aerosol dynamics. The situation becomes simplified, somewhat, when we have further knowledge of Δ and θ.

Although it is not explicitly stated, Equation (3.1) applies to the case in which an initial number of particles, N_o, are inserted into the system at time t = 0. The concentration at subsequent times is given by

$$N = \frac{N_o}{1 + N_o \tau/2} \quad , \tag{3.7}$$

where

$$\tau = \int_0^t \eta(\tau') \, dt' \quad . \tag{3.8}$$

Equations (3.7) and (3.8) are deceptively simple because they assume a knowledge of g(r, t). As we mentioned at the outset of Section 2, g(r, t) cannot be determined without solving the entire problem. However, estimates of the significant times scales involved in the coagulation process can be obtained by using approximate forms of g(r, t) or real-time measurements of g(r, t). It is through the latter that we consider turbulent coagulation in the context of the KOF.

In the remainder of this section, we will calculate the aerosol concentration as the particles emerge from a single well. The mathematical model developed for this case is directly applicable to the superplume, with the appropriate change of coordinates.

When the small-scale turbulent fluctuations are averaged out, the Eulerian equation for the aerosols is given by the extension of Equation (2.6) to now include convection. We have

$$\frac{\partial f(m)}{\partial t} + \nabla \bullet \left[\vec{U}\, f(m)\right] = \frac{1}{2} \int_{m_1} \int_{m_2} K(m_1, m_2)\, f(m_1)\, f(m_2)\, \delta(m - m_1 - m_2)\, dm_1\, dm_2 - f(m) \int_{m_2} K(m, m_2)\, f(m_2)\, dm_2 \quad , \tag{3.9}$$

where $\dot{U}$ is the average velocity and ∇ is the gradient operator. The right-hand side of Equation (3.9) is the same as that of Equation (2.6). For brevity, we have suppressed the explicit dependence of f on the space variable, $\vec{R}$, and on time, t. For example, f(m) is really $f(m, \vec{R}, t)$.

For an individual plume, Equation (3.9) is solved by matching the solution to the source emission at the origin (location of the burning well). If the source emission does not vary with time, Equation (3.9) will also be time invariant and, hence,

$$\frac{\partial f(m, \vec{R}, t)}{\partial t} = 0 \quad . \tag{3.10}$$

The space dependence of f(m), $\vec{R}$ is found by constructing a simplified geometric model of the plume as shown in Figure 3-2. In this figure, we approximate the plume as a tube of variable cross section, A(q), in which all the particles move with average velocity, $\dot{U}$, normal to the surface, A. The concentration is assumed to be uniform across the area. The coordinate system is constructed so that the q-axis is always directed along the direction of $\dot{U}$. If $|\vec{U}|$ is the magnitude of $\dot{U}$ along the q-axis, the divergence term in Equation (3.9) becomes

$$\nabla \bullet \left[\vec{U}\, f(m, \vec{R})\right] = \frac{\partial}{\partial q} \left[U(q)\, f(m, q)\right] \tag{3.11}$$

since, by construction, f(m, q) does not vary in directions normal to q.

We now let

$$f(m, q) = N(q)\, \phi(m, q) \quad , \tag{3.12}$$

where N(q) is the aerosol concentration (cm^{-3}) and $\phi(m, q)$ is the NMDF (expressed as a function of the space coordinate, q, instead of a function of time).

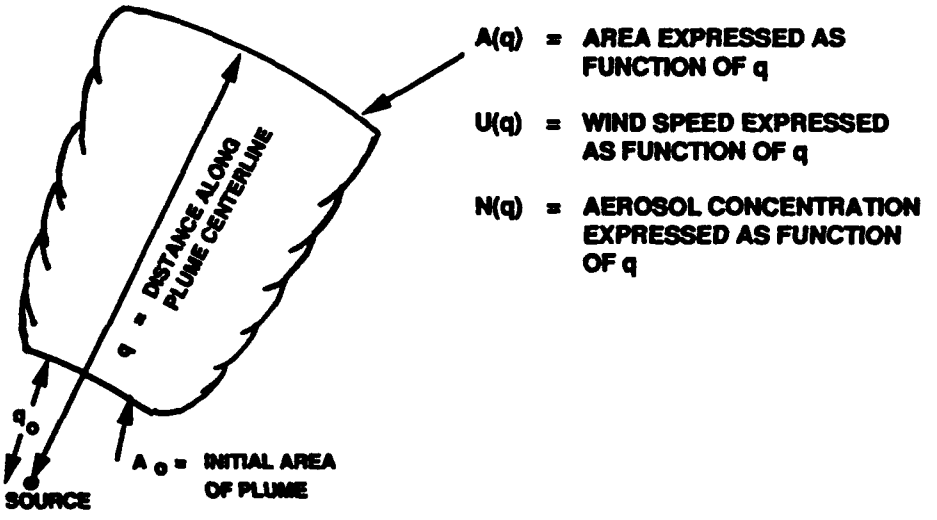

Figure 3-2. Model for individual plume.

Using Equations (3.10) and (3.11) in Equation (3.9) and then integrating over mass space using the techniques developed in Section 2 gives

$$\frac{\partial}{\partial q}(\mathrm{ANU}) = \frac{-(\mathrm{ANU})}{\mathrm{U}\,T(q)} \quad , \tag{3.13}$$

where the q-dependent time "constant," T(q), is given by

$$T(q) = \frac{2}{N(q)\,\eta(q)} \tag{3.14}$$

and

$$\eta(q) = \int_{r_1}\int_{r_2} K\left[m_1(r_1)\,m_2(r_2)\right] g(r_1,q)\,g(r_2,q)\,dr_1 dr_2 \quad . \tag{3.15}$$

The expressions for η corresponding to turbulent shear and turbulent inertial coagulation are given by Equations (3.3) and (3.5), respectively. As in Section 2, we have also introduced an NPRF, g(r, q), through the transformation

$$\phi(m, q)\,dq = g(r, q)\,dr \quad . \tag{3.16}$$

Further simplification is possible by using the conservation of mass. Multiplying Equation (3.9) by m and then integrating over mass space and area gives

$$\frac{\partial}{\partial q}\left(U(q)\,\overline{M}(q)\,A(q)\right) = 0 \quad , \tag{3.17}$$

where $\overline{M}(q)$ is the mass per cm^3. Equation (3.17) is analogous to Equation (2.10). $U\overline{M}A$ is the total mass emission rate (g s^{-1}) from a burning well, and as long as the flux tube of Figure 3-2 encompasses all the mass, we must have the equality

$$U(q)\,\overline{M}(q)\,A(q) = R_m \quad , \tag{3.18}$$

where R_m is the mass emission rate from the well expressed in g s^{-1}.

The next step in determining N(q) is to evaluate A(q). We assume a circular plume with radius, R_o, and area,

$$A(q) = \pi R_o^2(q) \quad . \tag{3.19}$$

R_o^2 is approximated by the equation

$$R_o^2 = 2 \int_0^t D(t')\,dt' \quad , \tag{3.20}$$

where D is the turbulent diffusion constant evaluated along the path. Following basic theoretical arguments discussed by Tennekes and Lumley (Ref. 14), we assume the relationship

$$D(t) \sim R_o(t)\,U(t) \quad , \tag{3.21}$$

which applies for times long enough for many independent eddies to establish fully developed turbulence.

With this assumption, Equation (3.20) can be written as a precise equation:

$$D = a\,R\,U \quad , \tag{3.22}$$

where "a" is an experimentally deduced constant, as yet undetermined. Inserting Equation (3.21) into Equation (3.20) and differentiating the latter gives

$$\frac{dR_o}{dt} = a\,U(t) \quad . \tag{3.23}$$

Integrating Equation (3.23) along the path yields

$$R_o(q) = a \int_0^t U(t)\, dt = a\, q \quad . \tag{3.24}$$

For the turbulent diffusion case considered, the radius of the plume is observed to be proportional to the distance traveled.[2]

In the regions described by Equation (3.21), it is recognized that Equation (3.24) is an approximation since the diffusion rates for horizontal and vertical diffusion are different. For the KOF, it has been observed that the plumes are typically constrained between 1 and 3 km in thickness. When the top of plume slows its rise and stabilizes from the initial buoyancy effect, the path variable q can be replaced by the horizontal axis in the direction of flow, x; the vertical dimension can be replaced by a constant value, $\Delta h \simeq 2$ km; and the horizontal dimension normal to the flow can be allowed to grow at a turbulent diffusion rate given by

$$y = b\, x \ , \tag{3.25}$$

where b is another experimentally deduced quantity. If it is desired, the approximation for A(q) could be improved by using real-time KOF experimental data.

However, until such KOF experimental data become available, we will use the circular model described by Equation (3.24) with the constant "a" determined from previous experimental data. Figure 3-3 shows the horizontal mean cloud half-width, $\sigma_y(x)$, for a stack plume as a function of downwind distance, x, from the source (Refs. 15, 16). Lines A through F correspond to different levels of stability. Taking the "average" of the curves gives the approximate relationship

$$\sigma_y = 0.1\, x \quad . \tag{3.26}$$

Identifying the σ_y and x of Equation (3.26) with the R_o and q, respectively, of Equation (3.24) gives

$$R(q) = 0.1\, q \tag{3.27}$$

and

$$A(q) = \pi R^2 = 3.14 \times 10^{-2}\, q^2 \ \text{cm}^2 \tag{3.28}$$

---

[2] I. Sykes (Ref. 13) has pointed out that the linear behavior of Equation (3.24) is an "early time" result but may well extend to dimensions near global scales. For very long transport times, the horizontal growth will vary with the square root of the distance.

during the initial stages of plume growth from the burning well. For numerical simplicity, the path length can be measured in kilometers instead of centimeters. We therefore write $q = 10^5 q_k$, where q_k is the distance in kilometers from the source, and use the equation

$$A(q) = 3.14 \times 10^8 \, q_k^2 \quad . \tag{3.29}$$

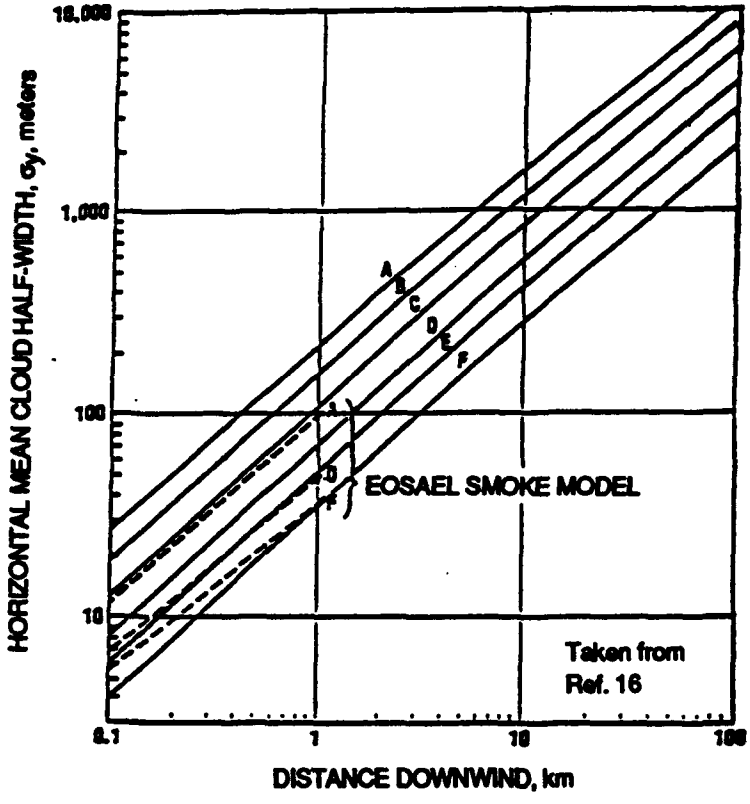

Figure 3-3. Horizontal mean cloud half-width $\sigma_y(x)$ for stack plumes as a function of downwind distance from the source (Source: Ref. 16).

We now write $U = 28 \, U_w$, where U_w is the windspeed in km/hr, and insert Equation (3.29) into Equation (3.18) to obtain

$$\overline{M} = \frac{(1.14) \times 10^{-10} \, R_m}{U_w q_k^2} \quad . \tag{3.30}$$

At this point, it is interesting to estimate the mass densities calculated from Equation (3.30) for an "average" burning well and compare them with the values used by

Porch (Ref. 7). If R_M is the aerosol emission rate for all the burning wells and W is the total number of burning wells, then the average mass emission rate per well, $\overline{R}_m$, is

$$\overline{R}_m = R_M/W \ \ g\,s^{-1} \quad . \tag{3.31}$$

We do not currently have information regarding the maximum emission rates for the largest individual fires, and there appears to be some uncertainty regarding both the total emission rate, R_M, and the average emission rate. Bauer (Ref. 1) has estimated R_M to be 45,000 metric tons per day, while Hobbs and Radke (Ref. 5) have estimated R_M to be 3,400 metric tons per day. However, it is not clear whether these numbers apply to the same number of burning wells and other similar conditions. For lack of more complete information, we take the average of the two references and use an emission rate of 24,000 metric tons per day, which converts to $R_M = 2.8 \times 10^5$ g s^{-1}. If we assume that 300 wells are burning,[3] the average emission rate per well is

$$\overline{R}_m = \frac{2.8 \times 10^5 \ g\,s^{-1}}{300} = 930 \ g\,s^{-1} \quad . \tag{3.32}$$

We may anticipate that all wells will not be burning at the same rate and that some wells may have an emission rate far exceeding that given by Equation (3.32).

In order to examine a hypothetical "worst-case" scenario, we use a value of $R_m^* = 9.3 \times 10^3$ g s^{-1} in the calculations, which is an order of magnitude higher than the average of Equation (3.32). At a distance of 1 kilometer from the well ($q_k = 1$), with a windspeed of 10 km/hr ($U_w = 10$) and well emission rate $R_m = R_m^* = 9.3 \times 10^3$ g s^{-1}, the mass density, $\overline{M}$, equals 1.06×10^{-7} g cm^{-3}, which is a factor of 2.12 higher than the maximum value of 5×10^{-8} g cm^{-3} used by Porch (Ref. 7). For the same values of q_k and U_w, but with $R_m = R_m^* = 930$ g s^{-1}, $\overline{M} = 1.06 \times 10^{-8}$ g cm^{-3}, which is consistent with Porch's (Ref. 7) range of interest, 5×10^{-9} to 5×10^{-8} g cm^{-3}. Using $U_w = 10$, $R_m = R_m^*$, but this time using $q_k = 10$, gives $\overline{M} = 1.06 \times 10^{-9}$ g cm^{-3}, which is a factor of 4.7 lower than Porch's (Ref. 7) minimum of 5×10^{-9} g cm^{-3}. The net result of this discussion is the reassuring observation that the values of $\overline{M}$ calculated for a realistic range of conditions are consistent with the values previously considered in a large forest fire.

We now return to the main thrust of this section, which is the determination of aerosol density, N(q), from Equation (3.13). Using the result

---

3 In the May/June 1991 time period, it is estimated that between 500–600 wells were burning.

$$\overline{M} = N(q)\,\overline{m}(q) = \frac{4\pi\rho}{3} N(q)\,\overline{r^3(q)} \tag{3.33}$$

in Equation (3.18) gives

$$N(q) = \frac{3R_m}{4\pi\rho\,\overline{r^3}\,AU} \quad . \tag{3.34}$$

Substituting Equation (3.34), in conjunction with the expressions for $\eta(q)$ obtained from Equations (3.3) and (3.5), respectively, in Equation (3.14) gives the following expressions for T(q) for *turbulent shear (T_S)* coagulation and *turbulent inertial (T_I)* coagulation:

$$T_S(q) = \frac{8\pi\rho\,AU\tau_k}{7.8\,R_m\,f_s} \quad , \tag{3.35}$$

where

$$f_s = 1 + \Delta \quad , \tag{3.36}$$

and

$$T_I(q) = \frac{6\rho_A\,\tau_k\,\lambda_k\,AU}{R_m\,r_I} \quad , \tag{3.37}$$

where

$$r_I = \frac{\overline{r^4}\,(1-\theta)}{\overline{r^3}} \quad . \tag{3.38}$$

Using either of the expressions $T_S(q)$ or $T_I(q)$ for T(q) in Equation (3.13) yields the density along the path. Solving Equation (3.13) for "ANU" gives

$$N(q) = \left(\frac{A_o\,N_o\,U_o}{U(q)\,A(q)}\right) \Gamma_c \quad , \tag{3.39}$$

where

$$\Gamma_c = e^{-\Lambda(q)} \tag{3.40}$$

and

$$\Lambda(q) = \int_{q_o}^{q} \frac{dq'}{U(q')\,T(q')} \quad . \tag{3.41}$$

The initial values A_o, N_o, and U_o are taken at the location q_o, where the approximation of Equation (3.27) is valid or, equivalently, where the initial jetting action and buoyancy effects of the well are dissipated. That is, our turbulent diffusion model only considers those effects attributed to usual atmospheric processes.

For the purposes of this analysis, we must make an assumption about the way $U(q')$, and $T(q')$ are treated in the integration of Equation (3.41). Until experimental data become available, we approximate these quantities as "path-averaged" constants. On the other hand, we do include the variation of A(q) from Equation (3.27). The results for *turbulent shear (S)* coagulation and *turbulent inertial (I)* coagulation are as follows:

$$\Lambda_S = \frac{l_S}{q_o} - \frac{l_S}{q}, \tag{3.42}$$

where

$$l_S = \frac{10\,R_m\,f_s}{U^2\,\tau_k\,\rho} \quad , \tag{3.43}$$

and

$$\Lambda_I = \frac{l_I}{q_o} - \frac{l_I}{q} \quad , \tag{3.44}$$

where

$$l_I = \frac{5.3\,R_m\,r_I}{\rho_A\,\tau_k\,\lambda_k\,U^2} \quad . \tag{3.45}$$

In the absence of coagulation, the spatial distribution of density is given by

$$N_1(q) = \frac{A_o\,N_o\,U_o}{U(q)\,A(q)} \quad . \tag{3.46}$$

This spreading behavior of the plume is attributed to atmospheric diffusion. $N_1(q)$ can be estimated from the mass ejection using the equation

$$\overline{M} = \overline{m}\,N \tag{3.47}$$

in Equation (3.18). The result is

$$N_1(q) = \frac{R_m}{\overline{m}\, U(q)\, A(q)} \quad . \tag{3.48}$$

$N_1(q)$ is the particle density that would exist in the absence of coagulation. Since $\Gamma_c \leq 1$, coagulation reduces the aerosol concentration beyond ordinary geometric dilution. Coagulation is quantitatively manifested by the parameters l_S or l_I, which pertain to turbulent shear coagulation and turbulent inertial coagulation, respectively. If we temporarily let $l = l_S$ or l_I, then the coagulation contribution to density can be written as

$$\Gamma_c = \exp -\left[\left(l/q_o - l/q \right) \right] \quad , \tag{3.49}$$

which is observed to be less than or equal to unity for the prescribed range $q \geq q_o$. The density at q_o is

$$N(q_o) = N_1(q_o) = \frac{R_m}{\overline{m}\, U(q_o)\, A(q_o)} \quad . \tag{3.50}$$

It is difficult to theoretically predict q_o since the processes describing the aerosol behavior as the oil emerges from the well are extremely complex. However, estimates of q_o can be obtained from visual observations. While a knowledge of q_o is required for determining the absolute level of aerosol concentration for $q \geq q_o$, it does not appear to be a critical factor in determining whether to consider coagulation effects when interpreting transport behavior. What is important is the spatial variation of Γ_c as a function of q when compared to other transport processes.

It is now worthwhile to examine certain features of N(q), including predictions of aerosol density close to the source and the apparent limiting effects of coagulation. Based on crude visual interpretations of the KOF photographs, we estimate the initiation of "conventional" atmospheric diffusion processes to begin between 0.1 and 1.0 kilometers from an individual burning well. For orientation, we compute $N_1(q_o)$ at $q_o = 10^5$ cm (1 km) for a windspeed U_w = 10 km hr^{-1}, for $R_m = R_m^*$, and for the average mass, $\overline{m} \left[\overline{m} = \left(4\pi\rho\, \overline{r^3}/3 \right) = 6.7 \times 10^{-13} \text{ g} \right]$, as determined from the size distribution defined by Equation (A.6) of the Appendix. Inserting these values in Equation (3.48) gives N_1 (at 1 km) = 1.6×10^5 particles per cm^3. This value of density appears to be consistent with the results of Hobbs and Radke (Ref. 5) at close-in ranges.

As a matter of theoretical interest, it is worthwhile to examine the behavior of aerosol density as a function of emission rate, R_m. By the way of example, we evaluate the asymptotic behavior of N(q). In the limit where $q >> l$ and $q \geq q_o$, the coagulation function Γ_c approaches the constant $\Gamma_c' = \exp(-l/q_o)$. From Equations (3.43) and (3.45), we note that both l_S and l_I are proportional to R_m. Therefore,

$$l = \alpha R_m \ , \tag{3.51}$$

where α is the proportionality constant [for example, $\alpha = (5.3\, r_I/\rho_A \tau_k \lambda_k U^2)$ in the case of turbulent inertial coagulation]. Substituting Equation (3.51) into Γ_c' yields the following result for the asymptotic behavior:

$$N_{as} = \left(\frac{R_m}{\overline{m}\, U(q)\, A(q)}\right) \exp\left[-R_m/\lambda\right] \ , \tag{3.52}$$

where

$$\lambda = q_o/\alpha \ . \tag{3.53}$$

Keeping all other factors the same, N_{as} has a maximum with respect to R_m. This maximum results from the competing factors of increased emission and reduction by coagulation. N_{as} maximizes at $R_m = 1$, with the maximum value given by

$$(N_{as})_{max} = \frac{(0.37)\,\lambda}{\overline{m}\, U(q)\, A(q)} \ . \tag{3.54}$$

As we indicated earlier, the main issue regarding the relevance of turbulent coagulation is to examine its effect on the interpretation of transport behavior. More specifically, we want to ensure that N(q) does not change appreciably due to turbulent coagulation over distances that are significant in the interpretation of transport. This means that we would like the function Γ_c to remain essentially constant. This condition is examined most easily by plotting Γ_c as a function of q with q_o and l as parameters.

To obtain an estimate of values of l that are of interest, we calculate l_S and l_I for the following set of parameters[4]:

$$R_m = R_m^* = 9.3 \times 10^3 \text{ g s}^{-1} \tag{a}$$

$$\rho = 1 \text{ gm cm}^{-3} \tag{b}$$

---

[4] Improved values for these parameters will be available when the measured KOF data are consolidated.

$$U = 278\ \text{cm s}^{-1}\left(U_w = 10\ \text{km hr}^{-1}\right) \quad \text{(c)}$$

$$f_s = 1 \quad \text{(d)}$$

$$\tau_k = 4.6\times10^{-3}\ \text{s}\left(\text{for } \varepsilon = 8{,}000\ \text{cm}^2\ \text{s}^{-3}\right) \quad \text{(e)}$$

$$\lambda_k = 2.8\times10^{-2}\ \text{cm}\left(\text{for } \varepsilon = 8{,}000\ \text{cm}^2\ \text{s}^{-3}\right) \quad \text{(f)}$$

$$\rho_A = 10^{-3}\ \text{g cm}^{-3} \quad \text{(g)}$$

$$r_I = 10^{-2}\ \text{cm} \quad \text{(h)} \qquad (3.55)$$

Inserting these values into Equations (3.43) and (3.45) gives

$$l_S = 2.6\ \text{m} \qquad (3.56)$$

and

$$l_I = 0.49\ \text{km} \ . \qquad (3.57)$$

For the conditions of Equation (3.55), the small value of l_S indicates that turbulent shear coagulation will not be a factor in transport since Γ_c is essentially constant at $\Gamma_c \simeq 1$ for all values of q of interest. Moreover, it is hard to imagine a set of realistic parameters that could change the foregoing conclusion.

On the other hand, Equation (3.57) shows that l_I is in the kilometer range. Considering the approximations and the unknown factors that have gone into the calculation of l_I, it is not inconceivable that l_I could be as high as 10 km under some set of circumstances. This could have an impact on the selection and interpretation of data used for transport predictions. Turbulent coagulation will have an effect on the prediction and interpretation of concentration if Γ_c varies significantly over the range of interest.

The precise criterion about what constitutes an acceptable degree of spatial variation remains to be defined for the Kuwaiti Oil Fire Field Experiment (KOFFE). From the analytical form of Γ_c [Equation 3.49)], there will be some minimum value of q, defined as q_{min}, beyond which variations of Γ_c with q will be very small. Moreover, since the dependence of Γ_c on q_o only affects the magnitude of concentration through the factor $\exp[-l/q_o]$, it follows that q_{min} will depend only on l.

John Cockayne (Ref. 17) has suggested a possible criterion for determining q_{min}. Cockayne's criterion is that turbulent coagulation will not be important in the range $q \geq q_{min}$ if we have the condition

$$\frac{\Gamma_c(2\,q_{min})}{\Gamma_c(q_{min})} \geq 0.9 \ , \tag{3.58}$$

where q_{min} is the distance beyond which $ln\ \Gamma_c$ changes by less than 10 percent over q_{min}.

Using Equation (3.49) in Equation (3.58), we easily deduce

$$1.1 \geq e^{l/2\,q_{min}} = 1 + l/2\,q_{min} \ , \tag{3.59}$$

which leads to the result

$$q_{min} \geq 5\,l \ . \tag{3.60}$$

Thus, if $l = l_I = 0.49$ km is used from Equation (3.57), we have $q_{min} = 2.45$ km. This value of q_{min} indicates that turbulent inertial coagulation ceases to be important for the average single well only 2.45 km downstream. On the other hand, if l_I is on the order of 10 km, then turbulent inertial coagulation could be very important at the formation of the superplume.

In the analytical model of this study, we have reduced the dependence of the spatial variation of turbulent coagulation to the two parameters q_o and l_I. Recognizing that there is some uncertainty in the numerical values of these quantities, it is instructive to visually examine the dependence of $\Gamma_c(q)$ on q_o and l_I. This will provide a preliminary indication of the range of values for q_o and l_I that may be important in assessment of transport issues. The results are shown in Figures 3-4 and 3-5. All of these curves begin at $q = q_o$.

Figure 3-4 shows the behavior of Γ_c as a function of q for assumed values of $q_o = 0.1$ km and $l_I = 0.01$, 0.1, and 1.0 km, respectively. As predicted, increasing the value of l_I for a fixed value of q_o leads to increasing reduction of the asymptotic value of Γ_c. When $(l_I/q_o) = 10$, the asymptotic value of Γ_c is less than 10^{-4} of its initial value. The case for $q_o = 0.1$ and $l_I = 10.0$ is not shown because the excessive reduction in aerosol density for this set of values diminishes interest in this calculation.

Figure 3-5 shows the behavior of Γ_c as a function of q for assumed values of $q_o = 1.0$ km and $l_I = 0.1$, 1.0, and 10.0 km. These results scale similarly to those in Figure 3-4 since the ratios of l_I/q_o are the same in each case. In addition, the respective

asymptotic values of $\Gamma_c = \exp - [l_l/q_o]$ are also equal. However, as shown in the latter set, the scale is stretched out and leads to significant changes in density extending into the tens-of-kilometers range.

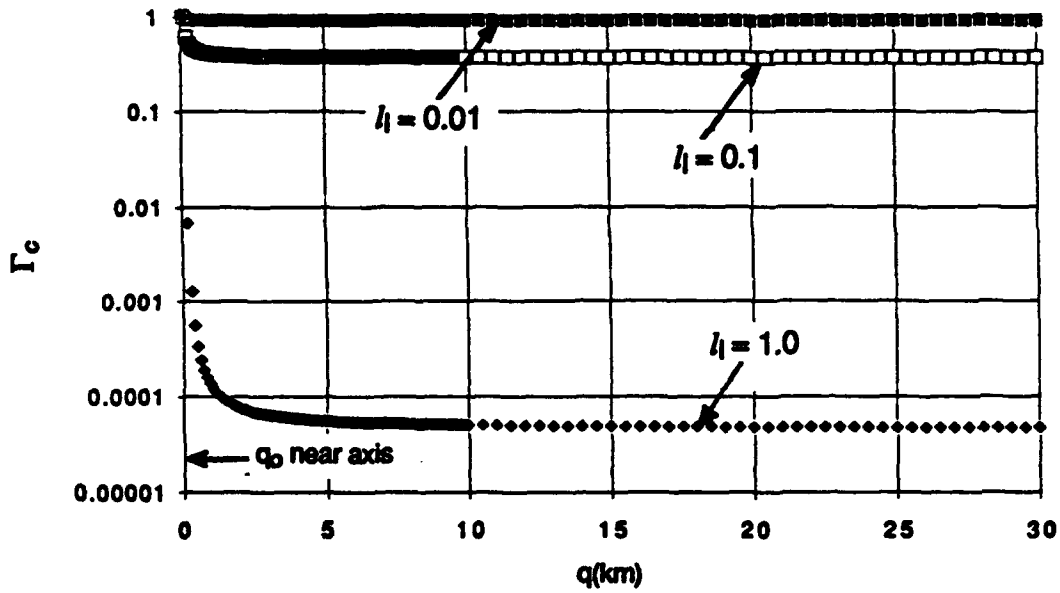

Figure 3-4. Γ_c as a function of q for q_o = 0.1 km with l_l as a parameter.

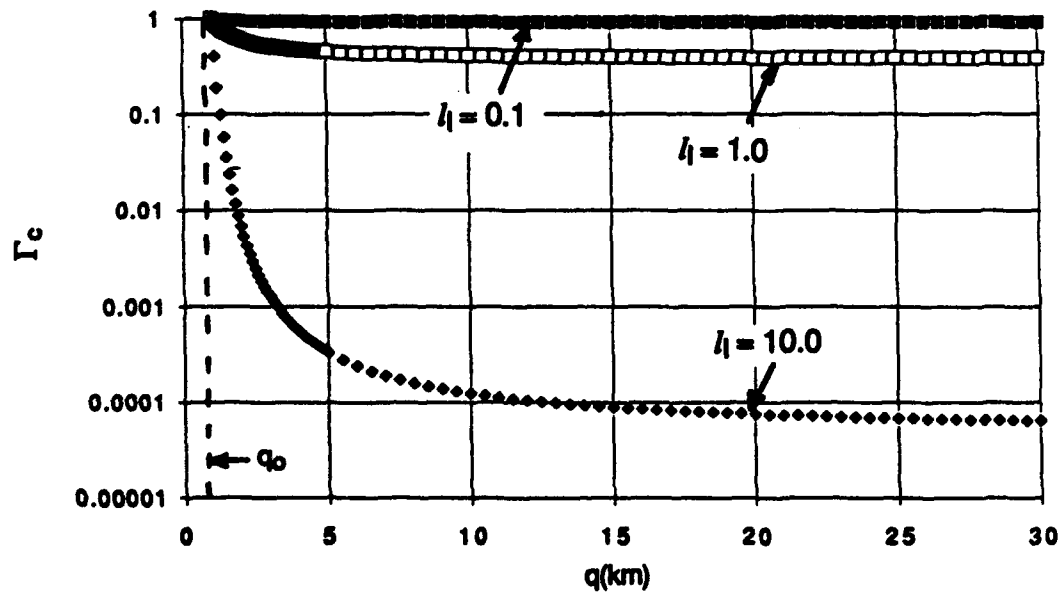

Figure 3-5. Γ_c as a function of q for q_o = 1.0 km with l_l as a parameter.

SECTION 4
CONCLUSION

In this paper, we focus on the KOF of 1991 to investigate one of several possible mass-changing processes that can limit the applicability of the current generation of transport codes, i.e., turbulent coagulation. The purpose of this paper is to make a preliminary assessment of the conditions where turbulent coagulation is or is not an important factor. Clearly, if airborne particles continue to coagulate in appreciable amounts during the transport phase, they cannot be unequivocally "tagged," and this potentially diminishes the validity of a transport calculation.

The approach is to develop an analytical formulation of the spatial behavior of aerosol density as the particles are carried along the turbulent wind field while simultaneously undergoing coagulation. Using approximations for the shape of the aerosol radial size distribution based on the large Canadian forest fire of 1950, we have been able to compute the time and space behavior of aerosol density for turbulent shear coagulation and turbulent inertial coagulation. The latter is nearly two orders of magnitude more effective than the former for the conditions of the KOF.

For a single source, the analysis shows that the upstream density can be written as $N = N_1 N_2$, where N_1 is that part due to ordinary atmospheric transport processes and N_2 is that part attributed to coagulation. N_2 depends on the source of emission, windspeed, atmospheric turbulence, and the characteristics of the coagulation process and behaves as $\exp(-l_I/q)$, where l_I is the characteristic dimension associated with coagulation and q is the upstream distance.

Using approximate numbers for the conditions of the KOF, l_I can range up to several kilometers and, in some cases, may be as large as 10 km. However, in the computation, there are a large number of unknown factors that can be determined from the experimental data. More accurate data would improve the estimate of the coagulation distance and, hence, define more precisely the regions where a self-consistent set of measurements can be integrated with valid transport models.

The theoretical models for the turbulent collection kernels are based on spherical shapes for the aerosol particles. In oil fires, however, the soot particles are usually not spherical but are more strand-like. Perhaps these particles can be better described using the theory of fractals.

Preliminary evaluation suggests that strand-like particles tend to interact more aggressively. In turn, this interaction would lead to a larger collection kernel that would manifest itself in a large l_I and would make turbulent coagulation an important factor in defining the spatial regions where transport codes can be compared with theoretical models.

Improvements to this initial theory should include fractal considerations and improved approximations for the aerosol size distribution function, turbulence levels, inhomogeneities within the plume, and collection efficiency.

SECTION 5
REFERENCES

1. E. Bauer, *Smoke Plumes from Kuwaiti Oil Fires as Atmospheric Experiment of Opportunity: An Early Look (U)*, Institute for Defense Analyses, IDA Document D-1059, October 1991. (UNCLASSIFIED)

2. D. Baumgardner, *Cloud Droplet Growth in Hawaiian Orographic Clouds (U)*, Ph.D. Thesis, University of Wyoming, 1988. (UNCLASSIFIED)

3. D.D. Evans et al., "In-Situ Burning of Oil Spills: Mesoscale Experiments," *Proceedings of the Fifteenth Arctic and Marine Oil Spill Program (U)*, Technical Seminar, June 10–12, 1992, Edmonton, Alberta. (UNCLASSIFIED)

4. G.W. Mulholland et al., "Cluster Size Distribution for Free Molecular Agglomera tion (U)," *Journal of Energy and Fuels*, **2**, 1988, pp. 481–486. (UNCLASSIFIED)

5. P.V. Hobbs and L.F. Radke, "Airborne Studies of the Smoke from the Kuwait Oil Fires (U)," *Science*, **256**, 1992, pp. 987–991. (UNCLASSIFIED)

6. D.W. Johnson et al., "Airborne Observations of the Physical and Chemical Characteristics of the Kuwait Oil Smoke Plume (U)," *Nature*, **353**, 1991, pp. 617–621. (UNCLASSIFIED)

7. W.M. Porch, "Blue Moons and Large Fires (U)," *Applied Optics*, **28**, 1989, pp. 1778–1784. (UNCLASSIFIED)

8. W.M. Porch, J.E. Penner, and D.A. Gillette, "Parametric Study of Wind Generated Super-μm Particle Effects in Large Fires (U)," *Atmos. Environ.*, **20**, 1986, pp. 919–929. (UNCLASSIFIED)

9. H.R. Pruppacher and J.D. Klett, *Microphysics of Clouds and Precipitation (U)*, D. Reidel Publishing, Chapter 12, 1978. (UNCLASSIFIED)

10. P.G. Saffman and J.S. Turner, "On the Collision of Drops in Turbulent Clouds (U)," *J. Fluid Mech.*, **1**, 1956, pp. 16–30. (UNCLASSIFIED)

11. L. Radke et al., *Airborne Monitoring and Smoke Characterization of Prescribed Fires on Forest Lands in Western Washington and Oregon (U)*, Environmental Protection Agency, Washington, DC, EPA 600/X-83-047, 1983, p. 122. (UNCLASSIFIED)

12. D. Baumgardner (National Center for Atmospheric Research), personal communi-cation. (UNCLASSIFIED)

13. I. Sykes (Atmospheric Research Associates of Princeton), personal communication. (UNCLASSIFIED)

14. H. Tennekes and J.L. Lumley, *A First Course in Turbulence (U)*, MIT Press, Chapter 1, 1972. (UNCLASSIFIED)

15. E. Bauer, *The Growth and Disappearance of Tracer Clouds in the Atmosphere (U)*, Institute for Defense Analyses, IDA Note N-890, June 1983. (UNCLASSIFIED)

16. D.B. Turner, *Workbook of Atmospheric Dispersion Estimates (U)*, USEPA, revised 1970. (UNCLASSIFIED)

17. J. Cockayne, (Science Applications International Corporation), personal communication. (UNCLASSIFIED)

APPENDIX
CALCULATION OF MOMENTS OF NORMALIZED PARTICLE RADIUS FUNCTION WHEN s = 3

When $r_U >> r_L$, the normalizing constant, A, is given by the approximation

$$A = (s-1)\, r_L^{s-1} \quad . \tag{A.1}$$

For s = 3, we obtain

$$A = 2\, r_L^2 \tag{A.2}$$

and, hence,

$$g(r) = \frac{2r_L^2}{r^3} \quad . \tag{A.3}$$

Using the fact that $r_U >> r_L$ gives the following results for the first four moments:

$$\bar{r} = A \int_{r_L}^{r_U} \frac{dr}{r^2} = 2\, r_L \tag{A.4}$$

$$\overline{r^2} = A \int_{r_L}^{r_U} \frac{dr}{r} = 2\, r_L^2 \, ln \, \frac{r_U}{r_L} \tag{A.5}$$

$$\overline{r^3} = A \int_{r_L}^{r_U} dr = 2\, r_L^2\, r_U \tag{A.6}$$

$$\overline{r^4} = A \int_{r_L}^{r_U} rdr = r_L^2\, r_U^2 \quad . \tag{A.7}$$

The values of $r_L = 2 \times 10^{-6}$ cm and $r_U = 2 \times 10^{-2}$ cm are used in all of the calculations.

DISTRIBUTION LIST

DNA-TR-93-171

DEPARTMENT OF DEFENSE

DEFENSE NUCLEAR AGENCY
2 CY ATTN: IMTS
2 CY ATTN: OPNA D TOOPS
2 CY ATTN: RAEM DR MUHAMMED OWAIS
ATTN: SPWE DR CHARLES GALLAWAY
ATTN: SPWE LTC MARK BYERS
ATTN: SPWE MAJ ROB COX

DEFENSE TECHNICAL INFORMATION CENTER
2 CY ATTN: DTIC/OC

OTHER GOVERNMENT

NATIONAL CENTER ATMOSPHERIC RESEARCH
ATTN: L RADKE

DEPARTMENT OF DEFENSE CONTRACTORS

INSTITUTE FOR DEFENSE ANALYSES
ATTN: D LEVINE
ATTN: E BAUER
ATTN: ED TOWNSLEY
ATTN: GEN L D WELCH
ATTN: H WOLFHARD
2 CY ATTN: I KOHLBERG
ATTN: IDA FILE
ATTN: L BIBERMAN
ATTN: N JORSTAD
ATTN: P ALBRIGHT
ATTN: P L MAJOR
ATTN: R GREENSTEIN
ATTN: R OLIVER
ATTN: R ROBERTS
ATTN: STD PUBLICATIONS

JAYCOR
ATTN: CYRUS P KNOWLES

KAMAN SCIENCES CORP
ATTN: DASIAC

KAMAN SCIENCES CORPORATION
ATTN: DASIAC

LOGICON R & D ASSOCIATES
ATTN: DOUGLAS C YOON

SCIENCE APPLICATIONS INTL CORP
ATTN: J COCKAYNE